

# 2D Cluster Mean Field Theory and Temperature: Spin-1 Bose Hubbard Model with Density Induced Tunnelling

A Dissertation for

Course code and Course Title: PHY-651 - Dissertation

Credits: 16

Submitted in partial fulfillment of Masters Degree

M.Sc. in Computational Physics

by

**MELIZA MARIA SOUZA**

Seat Number: 22P0430018

ABC ID: 835507299631

PRN: 20190243

Under the supervision of

**DR. RAMESH V. PAI**

School Of Physical and Applied Sciences

Physics Discipline



**GOA UNIVERSITY**

May 2024



Seal of the School

Examined by:

*R.V.*

## DECLARATION

I hereby declare that the data presented in this Dissertation report entitled, “2D Cluster Mean Field Theory and Temperature: Spin-1 Bose Hubbard Model with Density Induced Tunnelling” is based on the results of investigations carried out by me in the Physics Discipline at the School of Physical and Applied Sciences, Goa University under the Supervision of Dr. Ramesh V. Pai and the same has not been submitted elsewhere for the award of a degree or diploma by me. Further, I understand that Goa University or its authorities will be not be responsible for the correctness of observations/experimental or other findings given the dissertation.

I hereby authorize the University authorities to upload this dissertation on the dissertation repository or anywhere else as the UGC regulations demand and make it available to any one as needed.

Date: 08/05/2024

Place: Goa University

Name: Meliza Maria Souza

Seat Number: 22P0430018

Signature: 

COMPLETION CERTIFICATE

This is to certify that the dissertation report “2D Cluster Mean Field Theory and Temperature: Spin-1 Bose Hubbard Model with Density Induced Tunnelling” is a bonafide work carried out by Ms. Meliza Maria Souza under my supervision in partial fulfilment of the requirements for the award of the degree of Masters in the Discipline Physics at the School of Physical and Applied Sciences, Goa University.

Date: 08/05/2024

Name of the Supervising Teacher: Dr. Ramesh V. Pai

Signature:



Signature of Dean of the

School/Dept Stamp

School:

Date: 08/05/2024

Place: Goa University

## PREFACE

The Dissertation titled “2D Cluster Mean Field Theory and Temperature: Spin-1 Bose Hubbard Model with Density Induced Tunnelling” is an original work and is submitted in partial fulfillment of the Masters Degree in Science in Computational Physics at Goa University. The project was conducted under the supervision of Dr. Ramesh V. Pai at the School of Physical and Applied Sciences, Goa University, between June 2023 and May 2024.

## ACKNOWLEDGEMENT

I would like to express my sincere gratitude to my research guide Dr. Ramesh V. Pai, for his invaluable guidance and support throughout the project. Prof. Pai's insightful feedback, patience, and encouragement were instrumental in helping me navigate the complexities of this project.

I am extremely grateful to Dr. Bhargav K. Alavani for his invaluable mentorship and advice. His profound knowledge, encouragement and constructive feedback have been crucial in shaping my understanding of the subject and guiding me towards a successful outcome.

I would like to thank the faculty of the School of Physical and Applied Sciences, Goa University for providing an enriching academic environment and facilitating resources essential for this research endeavour. I sincerely acknowledge Dr. Elaine T. Dias for her support and encouragement throughout the thesis.

During the course of my thesis, I had the pleasure of working with Darshan T. Hosamani, Shantanu B. Naik, Pranjali A. Shet Verenkar, Ananya Mukherjee, Nashley A. Dias and Ramira Mascarenhas. Their encouragement, collaboration and shared enthusiasm have made this journey both fulfilling and memorable.

I express my deepest gratitude to my mom and dad for their unconditional love, support and encouragement throughout this journey. Their constant belief in my abilities has been a guiding light, and I am profoundly grateful for their sacrifices and unwavering dedication to my success. I would be remiss in not mentioning my grandmother, my beloved sister Apurva, Milbhor, Elsa, Aunt Rosy and my family for their support.

To my dear friend Azelia Fernandes, I owe a debt of gratitude for her constant support, kindness and inspiration. Her presence has brought joy and positivity to every step of this journey, and I am deeply thankful for her friendship.

Last but not the least, I would like to thank God for guiding me through every step of the way.

## ABBREVIATIONS

BEC	Bose-Einstein Condensate
BHM	Bose Hubbard Model
CMFT	Cluster Mean Field Theory
DIT	Density Induced Tunnelling
DMRG	Density Matrix Renormalization Group
EE	Entanglement Entropy
MC	Monte Carlo
MFT	Mean Field Theory
MI	Mott Insulator
MOT	Magneto-Optical Traps
NBL	Normal Bose Liquid
PSF	Polar Superfluid
QMC	Quantum Monte Carlo
RPA	Random Phase Approximation
SF	Superfluid

## ABSTRACT

The two-dimensional Spin-1 Bose Hubbard Model was studied using Cluster Mean Field Theory (CMFT) at finite temperatures with the inclusion of Density-Induced Tunnelling (DIT). The analyses were carried out with the aim of identifying the distinct phases such as polar superfluid (PSF), Mott Insulator (MI) and Normal Bose Liquid (NBL), and various magnetic properties that arise in the presence of spin-dependent antiferromagnetic interactions. The inclusion of density-induced tunnelling enhances the superfluid nature of bosons. The effect of density-induced tunneling on the critical on-site interaction  $U_0^C$  is studied at zero and finite temperatures. At a particular temperature, as the density-induced tunnelling amplitude increases, the superfluidity increases leading to a decrease in MI phase. However, at a given amplitude of density-induced tunnelling, as temperature increases, the Mott insulating phase increases.

# List of Figures

2.1	Illustration of the terms contained in the Spin-1 Bose-Hubbard Hamiltonian. (a) The single-atom tunnelling $t$ , (b) the on-site interaction $U_0$ , (c) the density-induced tunnelling $t'$ . . . . .	8
2.2	Clusters of size (a) $N_C = 1$ and (a) $N_C = 2$ . The black dots represent lattice sites and the blue solid line represents intra-cluster hopping. The blue dotted lines depict inter-cluster hopping approximated using mean-field theory. . . . .	13
3.1	Plots of (a) superfluid order parameters $\psi_\sigma$ , (b) individual density components $\rho_\sigma$ and (c) superfluid density $\rho_S$ and total density $\rho_{tot}$ versus the chemical potential $\mu$ for $U_2/U_0 = 0.03$ where $U_0 = 24.0$ and density-induced tunnelling strength $t' = 0$ . . . . .	18
3.2	Ground state energies $E_0$ against superfluid order parameters $\psi_1 = \psi_{-1}, \psi_0 = 0$ for 2D single-site ( $N_C = 1$ )near SF-MI transition (a) $\rho = 1$ and (b) $\rho = 2$ for $U_2/U_0 = 0.03$ where $U_0 = 24.0$ and density-induced tunnelling strength $t' = 0$ . Chemical potential $\mu$ increases from the blue to the red line across the phase transition. . . . .	18
3.3	Phase diagram plot for 2D single site without density-induced tunneling ( $t' = 0$ ) for $U_2/U_0 = 0.03$ . . . . .	19
3.4	Comparison plots of superfluid order parameters, individual density components and superfluid and total density versus the chemical potential $\mu$ for temperature $T = 0.05$ and $T = 0.1$ for $U_2/U_0 = 0.03$ where $U_0 = 24.0$ and density-induced tunnelling strength $t' = 0$ . . . . .	20
3.5	Finite temperature phase diagram plots for temperature (a) $T = 0.05$ and (b) $T = 0.1$ without density-induced tunneling ( $t' = 0$ ) for $U_2/U_0 = 0.03$ . . . . .	21

3.6	Chemical potential $\mu$ versus temperature $T$ plot with density-induced tunnelling amplitude $t' = 0$ for $U_2/U_0 = 0.03$ and $U_0 = 28.0$ . . . . .	22
3.7	Comparison plots of superfluid order parameters $\psi_\sigma$ , density-induced tunnelling order parameters $\eta_\sigma$ , boson densities $\rho_\sigma$ and superfluid density $\rho_S$ and total density $\rho_{tot}$ versus the chemical potential $\mu$ for two different density-induced tunnelling strengths $t' = 0.05$ and $t' = 0.1$ for $U_2/U_0 = 0.03$ where $U_0 = 24.0$ . . . . .	23
3.8	Superfluid density $\rho_S$ and total density $\rho_{tot}$ plotted against chemical potential $\mu$ for different density-induced tunnelling amplitudes for $U_2/U_0 = 0.03$ where $U_0 = 24.0$ . Insets focus on the MI region for $\rho = 1, 2$ . . . . .	24
3.9	Phase diagram plots for density-induced tunnelling amplitude (a) $t' = 0.05$ and (a) $t' = 0.1$ . . . . .	24
3.10	Effect of density-induced tunnelling amplitude $t'$ on the critical $U_0$ of Mott Insulator phases for $U_2/U_0 = 0.03$ . . . . .	25
3.11	Comparison plots of superfluid order parameters $\psi_\sigma$ , density-induced tunnelling order parameters $\eta_\sigma$ , boson densities $\rho_\sigma$ and superfluid density $\rho_S$ and total density $\rho_{tot}$ versus the chemical potential $\mu$ for two different density-induced tunnelling strengths $t' = 0.05$ and $t' = 0.1$ at temperature $T = 0.05$ for $U_2/U_0 = 0.03$ where $U_0 = 24.0$ . . . . .	26
3.12	Comparison plots of superfluid order parameters $\psi_\sigma$ , density-induced tunnelling order parameters $\eta_\sigma$ , boson densities $\rho_\sigma$ and superfluid density $\rho_S$ and total density $\rho_{tot}$ versus the chemical potential $\mu$ for two different density-induced tunnelling strengths $t' = 0.05$ and $t' = 0.1$ at temperature $T = 0.1$ for $U_2/U_0 = 0.03$ where $U_0 = 24.0$ . . . . .	27
3.13	Comparison plots of (a) superfluid density $\rho_S$ and (b) total density $\rho_{tot}$ versus the chemical potential $\mu$ for different density-induced tunnelling strengths at temperature $T = 0.05$ and $T = 0.1$ for $U_2/U_0 = 0.03$ where $U_0 = 24.0$ . Insets highlight the MI ( $\rho = 1$ ) phase for both temperatures $T = 0.05$ and $T = 0.1$ . . . . .	28
3.14	Chemical potential $\mu$ versus temperature $T$ plot with density-induced tunnelling amplitude $t' = 0.05$ for $U_2/U_0 = 0.03$ and $U_0 = 28.0$ . . . . .	29

3.15	Chemical potential $\mu$ versus temperature $T$ plot with density-induced tunnelling amplitude $t' = 0.1$ for $U_2/U_0 = 0.03$ and $U_0 = 28.0$ . . . . .	29
3.16	Phase diagram plots for $U_2/U_0 = 0.03$ at temperature $T = 0.05$ for density-induced tunneling amplitude (a) $t' = 0.05$ and (b) $t' = 0.1$ . . . . .	30
3.17	Phase diagram plots for $U_2/U_0 = 0.03$ at temperature $T = 0.1$ for density-induced tunneling amplitude (a) $t' = 0.05$ and (b) $t' = 0.1$ . . . . .	30
3.18	Effect of density-induced tunnelling amplitude $t'$ on the critical $U_0$ of Mott Insulator phases at finite temperature $T = 0.05$ and $T = 0.1$ for $U_2/U_0 = 0.03$ . . . . .	31
3.19	Plots of (a) superfluid order parameters $\psi_\sigma$ (b) individual density components $\rho_\sigma$ and (c) superfluid density $\rho_S$ and total density $\rho_{tot}$ versus the chemical potential $\mu$ for $U_2/U_0 = 0.03$ where $U_0 = 24.0$ and density-induced tunnelling strength $t' = 0$ for cluster size $N_C = 2$ . . . . .	32
3.20	Ground state energies $E_0$ against superfluid order parameters $\psi_1 = \psi_{-1}, \psi_0 = 0$ for 2D two site cluster ( $N_C = 2$ ) near SF-MI transition (a) $\rho = 1$ and (b) $\rho = 2$ for $U_2/U_0 = 0.03$ where $U_0 = 24.0$ . Chemical potential $\mu$ increases from the blue to the red line across the phase transition. . . . .	32
3.21	Plots of (a) singlet density $\rho_{SD}$ and nematic order parameter $Q^{z,z}$ and (b) local magnetic moment $\langle F^2 \rangle$ and cluster magnetic moment $\langle F_{TOT}^2 \rangle$ versus the chemical potential $\mu$ for $U_2/U_0 = 0.03$ where $U_0 = 24.0$ . . . . .	33
3.22	Rényi Entanglement Entropy $S_2$ for $U_2/U_0 = 0.03$ where $U_0 = 24.0$ . . . . .	33
3.23	Phase diagram plot for 2D two site cluster ( $N_C = 2$ ) without density-induced tunneling ( $t' = 0$ ) for $U_2/U_0 = 0.03$ . . . . .	34
3.24	Comparison plots of superfluid order parameters $\psi_\sigma$ individual density components $\rho_\sigma$ and superfluid density $\rho_S$ and total density $\rho_{tot}$ versus the chemical potential $\mu$ for temperatures $T = 0.2, T = 0.8$ and $T = 1.5$ for $U_2/U_0 = 0.03$ where $U_0 = 24.0$ and density-induced tunnelling strength $t' = 0$ . . . . .	35
3.25	Plots of (a) singlet density $\rho_{SD}$ and nematic order parameter $Q^{z,z}$ and (b) local magnetic moment $\langle F^2 \rangle$ and cluster magnetic moment $\langle F_{TOT}^2 \rangle$ versus the chemical potential $\mu$ for temperatures $T = 0.2, T = 0.8$ and $T = 1.5$ for density-induced tunnelling amplitude $t' = 0$ for $U_2/U_0 = 0.03$ and $U_0 = 24.0$ . . . . .	36

3.26	Chemical potential $\mu$ versus temperature $T$ plot with density-induced tunnelling amplitude $t' = 0$ for $U_2/U_0 = 0.03$ and $U_0 = 24.0$ . . . . .	37
3.27	Comparison plots of superfluid order parameters $\psi_\sigma$ , density-induced tunnelling order parameters $\eta_\sigma$ , boson densities $\rho_\sigma$ and superfluid density $\rho_S$ and total density $\rho_{tot}$ versus the chemical potential $\mu$ for two different density-induced tunnelling strengths $t' = 0.05$ and $t' = 0.1$ for $U_2/U_0 = 0.03$ where $U_0 = 24.0$ for cluster size $N_C = 2$ . . . . .	38
3.28	(a) Superfluid density $\rho_S$ and (b) total density $\rho_{tot}$ plotted against chemical potential $\mu$ for different density-induced tunnelling amplitudes for $U_2/U_0 = 0.03$ where $U_0 = 24.0$ . Insets focus on the MI phase corresponding to $\rho = 1$ and $\rho = 2$ . . . . .	39
3.29	Comparison plots of singlet density $\rho_{SD}$ , nematic order parameter $Q^{z,z}$ , local magnetic moment $\langle F^2 \rangle$ , cluster magnetic moment $\langle F_{TOT}^2 \rangle$ and Rényi EE $S_2$ against the chemical potential $\mu$ for density-induced tunnelling amplitude $t' = 0.05$ (left) and $t' = 0.1$ (right) for $U_2/U_0 = 0.03$ and $U_0 = 24.0$ . . . . .	40
3.30	Phase diagram plots for $U_2/U_0 = 0.03$ with density-induced tunnelling amplitude (a) $t' = 0.05$ and (a) $t' = 0.1$ for cluster size $N_C = 2$ . . . . .	41
3.31	Effect of density-induced tunnelling amplitude $t'$ on the critical $U_0$ of Mott Insulator phases for $U_2/U_0 = 0.03$ with cluster size $N_C = 2$ . . . . .	41
3.32	Comparison plots of superfluid order parameters $\psi_\sigma$ , density-induced tunnelling order parameters $\eta_\sigma$ , boson densities $\rho_\sigma$ and superfluid density $\rho_S$ and total density $\rho_{tot}$ versus the chemical potential $\mu$ for density-induced tunnelling strength $t' = 0.05$ at temperatures $T = 0.2$ , $T = 0.8$ and $T = 1.5$ for $U_2/U_0 = 0.03$ where $U_0 = 24.0$ . . . . .	42
3.33	Comparison plots of superfluid order parameters $\psi_\sigma$ , density-induced tunnelling order parameters $\eta_\sigma$ , boson densities $\rho_\sigma$ and superfluid density $\rho_S$ and total density $\rho_{tot}$ versus the chemical potential $\mu$ for density-induced tunnelling strength $t' = 0.1$ at temperatures $T = 0.2$ , $T = 0.8$ and $T = 1.5$ for $U_2/U_0 = 0.03$ where $U_0 = 24.0$ . . . . .	43

- 3.34 Comparison plots of (a) superfluid density  $\rho_S$  and (b) total density  $\rho_{tot}$  versus the chemical potential  $\mu$  for different density-induced tunnelling strengths at temperatures  $T = 0.2$ ,  $T = 0.8$  and  $T = 1.5$  for  $U_2/U_0 = 0.03$  where  $U_0 = 24.0$ . . . . . 44
- 3.35 Comparison plots of (a) singlet density  $\rho_{SD}$  and nematic order parameter  $Q^{z,z}$  and (b) local magnetic moment  $\langle F^2 \rangle$  and cluster magnetic moment  $\langle F_{TOT}^2 \rangle$  versus the chemical potential  $\mu$  for temperatures  $T = 0.2$ ,  $T = 0.8$  and  $T = 1.5$  for density-induced tunnelling amplitude  $t' = 0.05$  for  $U_2/U_0 = 0.03$  and  $U_0 = 24.0$ . . . . . 45
- 3.36 Comparison plots of (a) singlet density  $\rho_{SD}$  and nematic order parameter  $Q^{z,z}$  and (b) local magnetic moment  $\langle F^2 \rangle$  and cluster magnetic moment  $\langle F_{TOT}^2 \rangle$  versus the chemical potential  $\mu$  for temperatures  $T = 0.2$ ,  $T = 0.8$  and  $T = 1.5$  for density-induced tunnelling amplitude  $t' = 0.1$  for  $U_2/U_0 = 0.03$  and  $U_0 = 24.0$ . . . . . 46
- 3.37 Chemical potential  $\mu$  versus temperature  $T$  plot with density-induced tunnelling amplitude  $t' = 0.05$  for  $U_2/U_0 = 0.03$  and  $U_0 = 24.0$  for cluster size  $N_C = 2$ . . . . . 47
- 3.38 Chemical potential  $\mu$  versus temperature  $T$  plot with density-induced tunnelling amplitude  $t' = 0.1$  for  $U_2/U_0 = 0.03$  and  $U_0 = 24.0$  for cluster size  $N_C = 2$ . . . . . 47
- 3.39 Effect of density-induced tunnelling amplitude  $t'$  on the critical  $U_0$  of Mott Insulator phases at finite temperature  $T = 0.2$  for  $U_2/U_0 = 0.03$  for cluster size  $N_C = 2$ . . . . . 48

# List of Tables

3.1	The superfluid density and compressibility in the different phases of the Spin-1 Bose Hubbard model . . . . .	22
-----	---	----

# Contents

<b>List of Figures</b>	<b>v</b>
<b>List of Tables</b>	<b>x</b>
<b>1 Introduction</b>	<b>1</b>
1.1 Literature Review . . . . .	3
1.2 Motivation . . . . .	5
1.3 Objectives . . . . .	5
1.4 Overview . . . . .	6
<b>2 Methodology</b>	<b>7</b>
2.1 Introduction . . . . .	7
2.2 Mean Field Theory . . . . .	9
2.3 Cluster Mean Field Theory . . . . .	11
2.4 Finite temperature formalism . . . . .	14
2.4.1 Mean field theory . . . . .	14
2.4.2 Cluster Mean Field Theory . . . . .	15
<b>3 Results</b>	<b>17</b>
3.1 2D: Single Site . . . . .	17
3.1.1 Finite temperature . . . . .	20
3.1.2 Density-Induced Tunnelling . . . . .	22
3.1.3 Effect of finite temperature on Density-Induced Tunneling . . . . .	25
3.2 2D: Two site cluster . . . . .	31
3.2.1 Finite temperature . . . . .	35

*CONTENTS* xii

3.2.2 Density-Induced Tunneling . . . . . 37

3.2.3 Effect of finite temperature on Density-Induced Tunneling . . . . . 42

**4 Conclusion** **49**

**References** **51**

# Chapter 1

## Introduction

Bose-Einstein Condensation (BEC) is a quantum phenomenon in which a large number of bosons simultaneously occupy the ground state of a system. Bose-Einstein condensates were first conjectured theoretically in 1925 by Satyendra Nath Bose and were experimentally realized by Eric Cornell, Carl Wieman and Wolfgang Ketterle in 1995 when they produced BEC in a vapor of  $^{87}\text{Rb}$  atoms [3] and sodium atoms [11] respectively. Ever since, BEC has been realized in alkali atoms such as  $^7\text{Li}$  [8],  $^{39}\text{K}$  [33], Alkali Earth metals like  $^{40}\text{Ca}$  [30],  $^{84}\text{Sr}$  [41], Lanthanides  $^{168}\text{Er}$  [1],  $^{170}\text{Yb}$  [18], and binary mixtures such as  $^{87}\text{Rb} - ^{41}\text{K}$  [36]. Apart from these, spinor BEC like  $^{23}\text{Na}$  [40] has been observed in purely optical traps.

In condensed matter physics, in order to study interacting quantum particles, one needs to rely on quantum mechanics and statistical methods to predict the physical properties of the system. For this, the model Hamiltonian which includes interactions between particles and external perturbations is solved. Most of these models' Hamiltonian cannot be solved analytically, thus requiring some approximations. However, many times such methods predict a different result than actual outcomes and it becomes difficult to assess whether the approximations used are incorrect or the problem lies in the model Hamiltonian. Therefore, to overcome these shortcomings, a different approach is required by which the physical quantities of any system can be tuned in to test the modeled Hamiltonian and the methods used to solve it.

An important early contribution in this field came from the work of Jaksch et al. in

their 1998 paper titled “Cold Bosonic atoms in optical lattices” [25]. In this seminal work, Jaksch et al. laid the groundwork for the theoretical description of BECs in optical lattices using the Bose Hubbard Model. Their analysis focused on a fundamental quantum phase transition: the transformation from a superfluid state, where bosons flow coherently through the lattice, to a Mott Insulator state, where strong interactions localize the atoms at specific lattice sites. By tuning the depth of the optical potential, they explored ways to control this phase transition. This theoretical framework serves as foundation for numerous studies to understand how BEC behaves within these artificial periodic potentials. Soon after, Markus Greiner and Simon Fölling successfully loaded ultra-cold atoms in the optical lattice and observed the Mott insulating phase [20]. An optical lattice is a crystal structure of light, created by an interference of counter-propagating laser [10]. Ultra-cold atoms are trapped in a sinusoidal potential well created by a standing-wave laser beam in an optical lattice. Quantum tunnelling enables these atoms to delocalize across the entire lattice structure. In BEC, tunnelling dominates, resulting in a state of phase coherence between atoms occupying distinct lattice sites. However, increasing the potential depth hinders the tunnelling process. Energetically, it becomes unfavorable for atoms to tunnel into neighbouring sites. To minimize the system’s energy, a transition to a Mott Insulator (MI) state occurs, where each lattice site is singly occupied. In this state, the significantly reduced tunnelling effect leads to atom localization within their respective lattice sites, accompanied by a loss of phase coherence. This represents a Superfluid to Mott Insulator (SF-MI) phase transition.

The model which suitably describes the SF-MI phase transition is the Bose-Hubbard model (BHM) [17, 25]. This model can be solved using various methods like Mean-Field Theory (MFT) [17, 25], Cluster Mean-Field Theory (CMFT) [35], Monte Carlo (MC) simulations [5, 6, 31], Density Matrix Renormalization Group (DMRG) [16], Cluster Mean Field plus Density Matrix Renormalization theory (CMFT+DMRG) [19], Random Phase Approximation (RPA) [39] and the results obtained are in good agreement with the experiments. The Bose Hubbard Model has many extensions. Out of these, the Spin-1 Bose Hubbard Model shall be studied in the present work.

## 1.1 Literature Review

In experiments involving Bose-Einstein condensates (BECs), ultracold atoms are trapped within optical lattices providing a powerful platform for simulating intricate quantum many-body problems. Recent advancements in confining dilute alkali gases have revealed new opportunities for studying quantum magnetism. The behaviour of alkali atoms within traps is highly dependent on the trapping mechanism employed. Conventional magnetic traps, while effective for confinement, exhibit a significant drawback: they effectively suppress the intrinsic spin states of the trapped alkali atoms. This suppression renders the atoms, despite possessing inherent spin angular momentum, to behave like spinless, scalar particles. This limitation hinders the ability to exploit the full quantum complexity of these atomic systems, particularly the spinor nature of alkali Bose-Einstein condensates (BECs).

Conversely, purely optical traps [40] offer a paradigm shift. By manipulating light fields, these traps confine the atoms without significantly perturbing their internal spin states. Unlike the atoms prepared in Magneto-Optical Traps (MOT) that freeze the spin degrees of freedom, in purely optical traps these spins are free and the alkali BECs formed at low temperatures can retain their spinor nature. This has enhanced the interest in the study of quantum magnetism in confined dilute atomic gases.

Alkali atoms with nuclear spins  $I = 3/2$  such as  $^{23}\text{Na}$ ,  $^{39}\text{K}$  and  $^{87}\text{Rb}$  have hyper-fine spin  $F = 1$ . Thus, the interactions between these atoms is spin-dependent. Depending upon the scattering lengths of the singlet and quintuplet channels, the interactions are ferromagnetic (example  $^{87}\text{Rb}$ ) or anti-ferromagnetic (example  $^{23}\text{Na}$ ) [23]. This interaction allows the study of superfluidity and magnetism, and modifies the nature of the phase diagrams.

The Spin-1 Bose Hubbard model has been studied by many groups at zero temperature [29,32,37]. The phases arising in the model are similar to the spinless BHM. However, the superfluid phase can either be ferromagnetic or polar depending on the spin-dependent interaction. In the latter case, the SF-MI phase transition is continuous if the boson density  $\rho$  at a site is odd, however it is of first order if the boson density is even at a site. Finite temperature studies of the model were also carried by Pai et al [37]. In their study,

they observed that several of the SF-MI transitions are of first order and at sufficiently high temperatures, they become continuous via tri-critical points. Apart from the superfluid and MI phases, another phase, the Normal Bose Liquid (NBL) was observed in the same study at higher temperatures. It was noted that the MI-NBL phases are not distinct and are thus seen as a cross-over. The cross-over boundary values of compressibility  $\kappa = 0.01, 0.02$ , and  $0.03$  were chosen in their study. Another interesting observation was that the critical on-site interaction  $U_0^C$  decreases as temperature increases and MI phases grow at the expense of SF phase.

Furthermore, the Spin-1 Bose Hubbard Model was studied using Cluster Mean Field Theory (CMFT) by Alavani et al. [2]. The authors noted that the single-site Mean Field Theory neglects fluctuations in the SF and MI phases. This leads to an over-estimation of the critical on-site interaction  $U_0^C$ . Single-site MFT also fails to predict the magnetic nature of the different phases. Upon treating the intra-cluster hopping exactly in CMFT, the magnetic phases and SF-MI phases were studied. It was observed that for anti-ferromagnetic interaction ( $U_2 > 0$ ), the superfluid phase has polar symmetry. In addition to this, the odd density MI phase was nematic while the even density MI phase was nematic for small values of  $U_2$  or singlet for large values of  $U_2$ . The SF-MI phase transition noted a decrease in the critical on-site interaction  $U_0^C$  with cluster size.

A different extension of the BH model consists of adding terms where the hopping between two sites also depends on the two corresponding densities [15]. The effect of density-induced tunnelling has been studied on the Bose Hubbard Model by many groups [9, 14, 15, 27, 34, 43]. The main effect of density-induced tunnelling is to enhance superfluidity. It results in a shift of the critical hopping parameter for the SF-MI phase transition [9]. The density-induced tunneling term suppresses the MI region and this region is even more suppressed when the particle density  $n$  increases [43]. In their paper titled “Non-standard Hubbard models in optical lattices: a review,” Dutta et al. studied the inclusion of the density-induced tunnelling term on the Bose Hubbard Model. They noted that as a direct consequence of the density-induced tunneling, the critical point of the superfluid-Mott insulator transition is affected, depending on both the scattering length  $a_S$  and the filling factor  $n$ . The SF-MI transition is also significantly shifted towards lower values. The occupation-dependent nature is reflected by the fact that the Mott lobes with higher

filling factors  $n$  are more strongly affected. They observed that for a filling factor  $n$ , the generalized and standard Bose-Hubbard models differ by approximately  $(2n - 1)T$  at the tips of the Mott lobes (where  $T$  is density induced tunnelling amplitude) [15].

## 1.2 Motivation

Observing BEC and SF-MI transitions in optical lattices offers a new window into quantum phase transitions. With the advancement in experimental techniques, it is possible to study the spinor bosons in the optical lattice, which combines superfluidity and magnetism. The Spin-1 Bose Hubbard Model is one such fundamental system that captures the interplay of spin degrees of freedom, particle interactions, and hopping in ultracold atomic gases, providing insights into many interesting quantum phenomena. In the traditional framework of the Spin-1 Bose Hubbard Model, the density-induced tunnelling has not been studied yet and hence the focus stems from its potential to unveil new quantum phases and transitions. Despite the dominance of quantum effects in these phase transitions, small but finite thermal fluctuations are unavoidably present in experiments. This necessitates the development of theoretical frameworks that can incorporate both quantum and thermal fluctuations. These requirements motivate the present study.

## 1.3 Objectives

The objectives of the thesis are as follows:

- To develop a finite temperature cluster mean field theory for a two dimensional Spin-1 Bose Hubbard Model.
- To investigate the effect of the Density Induced Tunneling term on the behaviour of the Spin-1 Bose Hubbard Model.
- To study the influence of finite temperatures on the properties of the system.
- To identify and characterize the phase transitions induced by density induced hopping along with finite temperatures.

## 1.4 Overview

The thesis is organized in the following way.

Chapter 1 includes the introduction, background, aim and objectives, hypotheses and scope of the topic under study. It also delves into the literature review carried out during the course of the dissertation. Chapter 2 describes the methodology used to formulate the finite temperature cluster mean field theory for a two-dimensional Spin-1 Bose Hubbard model with density-induced tunneling. Chapter 3 comprises of the analyses, observations and results obtained upon studying the model. Chapter 4 summarizes and concludes the outcomes of the undertaken topic.

# Chapter 2

## Methodology

### 2.1 Introduction

The Hamiltonian for the Spin-1 Bose Hubbard model is defined as

$$\hat{H} = -t \sum_{\langle i,j \rangle, \sigma} (\hat{a}_{i,\sigma}^\dagger \hat{a}_{j,\sigma} + \hat{a}_{j,\sigma}^\dagger \hat{a}_{i,\sigma}) + \frac{U_0}{2} \sum_i \hat{n}_i (\hat{n}_i - 1) + \frac{U_2}{2} \sum_i (\vec{F}_i^2 - 2\hat{n}_i) - \mu \sum_i \hat{n}_i \quad (2.1)$$

where  $\langle i, j \rangle$  denotes the pairs of nearest neighbours in the lattice and the spin projection  $\sigma = -1, 0, 1$ .  $\hat{a}_{i,\sigma}$  ( $\hat{a}_{i,\sigma}^\dagger$ ) annihilates (creates) a boson in a hyperfine state  $m_F = \sigma$  at site  $i$ . The number of bosons located at a site  $i$  are represented by  $\hat{n}_i = \sum_\sigma \hat{n}_{i,\sigma}$  where  $\hat{n}_{i,\sigma} = \hat{a}_{i,\sigma}^\dagger \hat{a}_{i,\sigma}$ .  $\vec{F}_i = (F_i^x, F_i^y, F_i^z)$  is the spin operator at site  $i$  with  $F_i^\alpha = \sum_{\sigma,\sigma'} \hat{a}_{i,\sigma}^\dagger S_{\sigma,\sigma'}^\alpha \hat{a}_{i,\sigma'}$  where  $S^\alpha$  are the standard spin-1 matrices

$$S^x = \frac{1}{\sqrt{2}} \begin{pmatrix} 0 & 1 & 0 \\ 1 & 0 & 1 \\ 0 & 1 & 0 \end{pmatrix}, \quad S^y = \frac{i}{\sqrt{2}} \begin{pmatrix} 0 & -1 & 0 \\ 1 & 0 & -1 \\ 0 & 1 & 0 \end{pmatrix}, \quad S^z = \begin{pmatrix} 1 & 0 & 0 \\ 0 & 0 & 0 \\ 0 & 0 & -1 \end{pmatrix}$$

The term  $\vec{F}_i^2$  in the Hamiltonian using the above matrices becomes

$$\begin{aligned} \vec{F}_i^2 &= \hat{n}_1^2 + \hat{n}_{-1}^2 + \hat{n}_1 + \hat{n}_{-1} + 2\hat{n}_0 + 2\hat{n}_1\hat{n}_0 + 2\hat{n}_0\hat{n}_{-1} \\ &\quad - 2\hat{n}_1\hat{n}_{-1} + 2\hat{a}_1^\dagger \hat{a}_{-1}^\dagger \hat{a}_0^2 + 2\hat{a}_1 \hat{a}_{-1} \hat{a}_0^{\dagger 2} \end{aligned} \quad (2.2)$$

The first term in the Hamiltonian represents tunnelling of bosons between the nearest neighbour sites with hopping amplitude  $t$ , whereas the second term denotes on-site interaction among the bosons occupying the site. The energy due to spin configurations is represented by the third term, which penalizes non-zero spin configurations on individual sites. The interaction terms arise due to the difference in scattering lengths  $a_0$  and  $a_2$  for  $S_0$  and  $S_2$  channels respectively and are expressed as  $U_0 = \frac{4\pi\hbar^2(a_0+2a_2)}{3M}$  and  $U_2 = \frac{4\pi\hbar^2(a_2-a_0)}{3M}$  where  $M$  is the mass of the atom. The scattering lengths of  $^{23}\text{Na}$  are  $a_0 = 49.4a_B$  and  $a_2 = 54.7a_B$  where  $a_B$  is the Bohr radius and thus  $U_2 > 0$ . Similarly, the scattering lengths of  $^{87}\text{Rb}$  are  $a_0 = (110 \pm 4)a_B$  and  $a_2 = (107 \pm 4)a_B$ , resulting in  $U_2 < 0$  [23]. Lastly, the fourth term is the chemical potential that controls the number of bosons in the system.

The density-induced tunnelling term is an extension of the Bose Hubbard model where the probability of tunnelling to neighbouring sites depends on the two corresponding densities.

Upon adding the density-induced tunneling term to equation (2.1), the Hamiltonian reads

$$\begin{aligned} \hat{H} = & -t \sum_{\langle i,j \rangle, \sigma} (\hat{a}_{i,\sigma}^\dagger \hat{a}_{j,\sigma} + \hat{a}_{j,\sigma}^\dagger \hat{a}_{i,\sigma}) + \frac{U_0}{2} \sum_i \hat{n}_i(\hat{n}_i - 1) + \frac{U_2}{2} \sum_i (\vec{F}_i^2 - 2\hat{n}_i) - \mu \sum_i \hat{n}_i \\ & - t' \sum_{\langle i,j \rangle, \sigma} (\hat{a}_{i,\sigma}^\dagger (\hat{n}_{i,\sigma} + \hat{n}_{j,\sigma}) \hat{a}_{j,\sigma} + \hat{a}_{j,\sigma}^\dagger (\hat{n}_{i,\sigma} + \hat{n}_{j,\sigma}) \hat{a}_{i,\sigma}) \end{aligned} \quad (2.3)$$

where  $t'$  denotes the density-induced tunneling amplitude. The tunnelling and interaction terms in Hamiltonian (2.3) are illustrated in figure 2.1.

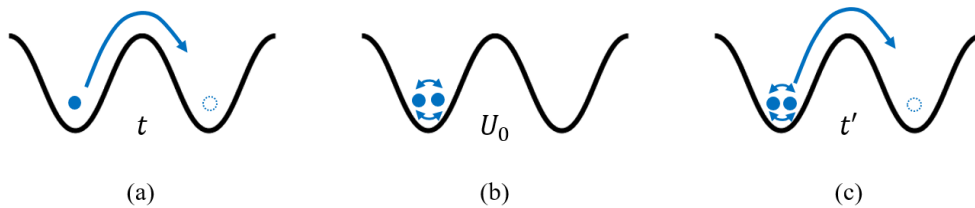


Figure 2.1: Illustration of the terms contained in the Spin-1 Bose-Hubbard Hamiltonian. (a) The single-atom tunnelling  $t$ , (b) the on-site interaction  $U_0$ , (c) the density-induced tunnelling  $t'$ .

The Spin-1 Bose Hubbard Hamiltonian with density-induced tunneling defined in equation (2.3) cannot be solved exactly due to the presence of the hopping terms. However, various techniques such as Mean-Field Theory [37], Cluster Mean-Field Theory [2], Quantum

Monte Carlo (QMC) simulations [4, 12], Variational Monte Carlo (MC) simulations [42], Density Matrix Renormalization Group (DMRG) [7, 22, 38] and analytical methods [13, 24] like Strong Coupling Expansion [28] are used to study the Hamiltonian. Out of these, the Mean-Field approach will be considered for this study which is described in the following section.

## 2.2 Mean Field Theory

Mean field theory has three formulations out of which the decoupling approximation will be used. The mean field approach is a suitable approximation for bosonic atoms in an optical lattice in order to qualitatively capture the allowed phases since majority of the atoms will be in the condensed state. As such, operators may be expressed as a sum of an average around some fluctuating operator and the small deviations or fluctuations representing uncondensed bosons.

Using this approximation, the hopping terms described in equation (2.3) are decoupled to obtain an effective single-site Hamiltonian which is then solved self-consistently. Following the mean-field decoupling, the annihilation and creation operators can be expressed as:

$$\begin{aligned}\hat{a}_{i,\sigma} &= \langle \hat{a}_{i,\sigma} \rangle + \delta \hat{a}_{i,\sigma} \\ \hat{a}_{i,\sigma}^\dagger &= \langle \hat{a}_{i,\sigma}^\dagger \rangle + \delta \hat{a}_{i,\sigma}^\dagger\end{aligned}\tag{2.4}$$

where  $\langle \mathcal{O} \rangle$  is the equilibrium value of the operator  $\mathcal{O}$  and  $\delta \mathcal{O}$  denotes small deviations. The crucial part of mean-field decoupling approximation lies in neglecting quadratic fluctuations, that is,  $\delta \hat{a}_{i,\sigma}^\dagger \delta \hat{a}_{j,\sigma} \approx 0$ .

Using the expressions defined in (2.4), the hopping term in (2.3) can be decoupled as

$$\hat{a}_{i,\sigma}^\dagger \hat{a}_{j,\sigma} \approx \langle \hat{a}_{i,\sigma}^\dagger \rangle \hat{a}_{j,\sigma} + \langle \hat{a}_{j,\sigma} \rangle \hat{a}_{i,\sigma}^\dagger - \langle \hat{a}_{i,\sigma}^\dagger \rangle \langle \hat{a}_{j,\sigma} \rangle\tag{2.5}$$

Since superfluid phases are expected, the superfluid order parameter with spin component  $\sigma$  is represented as  $\psi_\sigma \equiv \langle \hat{a}_{i,\sigma} \rangle \equiv \langle \hat{a}_{i,\sigma}^\dagger \rangle$  which is real. Homogeneity of the lattice makes order parameters site independent, that is,  $\psi_{i,\sigma} \equiv \psi_\sigma$ .

$$\hat{a}_{i,\sigma}^\dagger \hat{a}_{j,\sigma} \approx \psi_\sigma (\hat{a}_{i,\sigma} + \hat{a}_{i,\sigma}^\dagger) - \psi_\sigma^2\tag{2.6}$$

In a similar way, the density-induced tunneling term can be decoupled as follows:

$$\begin{aligned}\hat{n}_{i,\sigma}\hat{a}_{i,\sigma} &= \langle \hat{n}_{i,\sigma}\hat{a}_{i,\sigma} \rangle + \delta(\hat{n}_{i,\sigma}\hat{a}_{i,\sigma}) = \eta_{i,\sigma} + \delta(\hat{n}_{i,\sigma}\hat{a}_{i,\sigma}) \\ \hat{a}_{i,\sigma}^\dagger\hat{n}_{i,\sigma} &= \langle \hat{a}_{i,\sigma}^\dagger\hat{n}_{i,\sigma} \rangle + \delta(\hat{a}_{i,\sigma}^\dagger\hat{n}_{i,\sigma}) = \eta_{i,\sigma}^* + \delta(\hat{a}_{i,\sigma}^\dagger\hat{n}_{i,\sigma})\end{aligned}\quad (2.7)$$

where  $\eta_{i,\sigma} = \langle \hat{n}_{i,\sigma}\hat{a}_{i,\sigma} \rangle$  is the order parameter describing density-induced tunneling properties [26].

Applying the approximation described in (2.7), the DIT term can be expressed as

$$\begin{aligned}\hat{a}_{i,\sigma}^\dagger(\hat{n}_{i,\sigma} + \hat{n}_{j,\sigma})\hat{a}_{j,\sigma} &\approx \langle \hat{a}_{i,\sigma}^\dagger\hat{n}_{i,\sigma} \rangle\hat{a}_{j,\sigma} + \langle \hat{a}_{j,\sigma} \rangle\hat{a}_{i,\sigma}^\dagger\hat{n}_{i,\sigma} - \langle \hat{a}_{i,\sigma}^\dagger\hat{n}_{i,\sigma} \rangle\langle \hat{a}_{j,\sigma} \rangle \\ &+ \langle \hat{n}_{j,\sigma}\hat{a}_{j,\sigma} \rangle\hat{a}_{i,\sigma}^\dagger + \langle \hat{a}_{i,\sigma}^\dagger \rangle\hat{n}_{j,\sigma}\hat{a}_{j,\sigma} - \langle \hat{n}_{j,\sigma}\hat{a}_{j,\sigma} \rangle\langle \hat{a}_{i,\sigma}^\dagger \rangle\end{aligned}\quad (2.8)$$

Simplifying further, the term above can be expressed as

$$\hat{a}_{i,\sigma}^\dagger(\hat{n}_{i,\sigma} + \hat{n}_{j,\sigma})\hat{a}_{j,\sigma} \approx \eta_\sigma(\hat{a}_{i,\sigma}^\dagger + \hat{a}_{i,\sigma}) + \psi_\sigma\hat{a}_{i,\sigma}^\dagger\hat{n}_{i,\sigma} + \psi_\sigma\hat{n}_{i,\sigma}\hat{a}_{i,\sigma} - 2\psi_\sigma\eta_\sigma \quad (2.9)$$

Employing the expressions obtained in (2.6) and (2.9), the mean-field Hamiltonian is

$$\hat{H} = \sum_i \hat{H}_i^{MF} \quad (2.10)$$

where

$$\begin{aligned}H_i^{MF} &= -zt \sum_\sigma (\psi_\sigma(\hat{a}_{i,\sigma} + \hat{a}_{i,\sigma}^\dagger) - \psi_\sigma^2) \\ &+ \frac{U_0}{2} \sum_i \hat{n}_i(\hat{n}_i - 1) + \frac{U_2}{2} \sum_i (\vec{F}_i^2 - 2\hat{n}_i) - \mu \sum_i \hat{n}_i \\ &- zt' \sum_\sigma (\eta_\sigma(\hat{a}_{i,\sigma}^\dagger + \hat{a}_{i,\sigma}) + \psi_\sigma\hat{a}_{i,\sigma}^\dagger\hat{n}_{i,\sigma} + \psi_\sigma\hat{n}_{i,\sigma}\hat{a}_{i,\sigma} - 2\psi_\sigma\eta_\sigma)\end{aligned}\quad (2.11)$$

where  $z$  denotes the number of nearest neighbours.

The superfluid order parameters  $\psi_\sigma$  for  $\sigma = -1, 0, 1$  are computed iteratively using a self-consistent method. This iterative procedure begins with an initial guess for  $\{\psi_1, \psi_0, \psi_{-1}\}$  and  $\{\eta_1, \eta_0, \eta_{-1}\}$ . The single-site mean-field Hamiltonian (2.11) is constructed in the Fock basis  $|n_1, n_0, n_{-1}\rangle$  for which the total number of bosons allowed to occupy a site are truncated at a finite value  $n_{max}$ . Upon diagonalizing the Hamiltonian, the eigenvalues

$E_\alpha$  and eigenvectors  $|\alpha\rangle$  are obtained. A new guess for  $\{\psi_1, \psi_0, \psi_{-1}\}$  and  $\{\eta_1, \eta_0, \eta_{-1}\}$  is calculated through the expectation value using the ground state eigenvector. This process is repeated until the values of  $\{\psi_1, \psi_0, \psi_{-1}\}$  and  $\{\eta_1, \eta_0, \eta_{-1}\}$  are converged and self-consistency condition is fulfilled.

The superfluid density,  $\rho_S$  and boson density,  $\rho$  are calculated using the self-consistent ground state eigenvector as follows:  $\rho_S = \sum_\sigma |\psi_\sigma|^2$  and  $\rho = \sum_\sigma \langle \hat{n}_\sigma \rangle$ . The Spin-1 Bose-Hubbard model exhibits distinct ground states characterized by the superfluid density,  $\rho_S$ . The Superfluid (SF) phase has finite  $\rho_S$ , indicating the presence of a delocalized and coherent bosonic state. Conversely, the Mott Insulator (MI) phase is characterized by  $\rho_S = 0$ , signifying the localization of bosons at lattice sites and the absence of superfluid flow.

Single-site MFT adopts a simplified approach, treating each lattice site independently. However it exhibits limitations in capturing the magnetic characteristics of different phases within the model and overestimates the interaction strength required for the SF-MI transition. This arises from the decoupling approximation, which weakens the effective interaction strength, leading to an inaccurate prediction of the phase boundary.

## 2.3 Cluster Mean Field Theory

Cluster mean-field theory (CMFT) offers a significant advancement over single-site mean-field theory for studying interacting systems. While both methods utilize mean-field approximations, CMFT provides a more accurate description of properties such as magnetic ordering, phase transitions, and critical points.

In cluster mean-field theory, the lattice is divided into clusters which are made up of  $N_C$  number of sites. The interactions within the cluster are treated exactly whereas the inter-cluster interactions are decoupled using standard mean-field decoupling approximations described in Section 2.2.

The Hamiltonian of the entire system can be written as a sum over all the cluster using expression (2.1) as

$$\hat{H} = \sum_{cluster} \hat{H}^{cluster} \quad (2.12)$$

where

$$\begin{aligned}
\hat{H}^{cluster} = & -t \sum_{\langle i,j \rangle, \sigma}^{N_C} (\hat{a}_{i,\sigma}^\dagger \hat{a}_{j,\sigma} + \hat{a}_{j,\sigma}^\dagger \hat{a}_{i,\sigma}) \\
& + \frac{U_0}{2} \sum_i^{N_C} \hat{n}_i (\hat{n}_i - 1) + \frac{U_2}{2} \sum_i^{N_C} (\vec{F}_i^2 - 2\hat{n}_i) - \mu \sum_i^{N_C} \hat{n}_i \\
& - t' \sum_{\langle i,j \rangle, \sigma}^{N_C} (\hat{a}_{i,\sigma}^\dagger (\hat{n}_{i,\sigma} + \hat{n}_{j,\sigma}) \hat{a}_{j,\sigma} + \hat{a}_{j,\sigma}^\dagger (\hat{n}_{i,\sigma} + \hat{n}_{j,\sigma}) \hat{a}_{i,\sigma}) \\
& - zt \sum_{i,\sigma}^{N_c} (\psi_\sigma (\hat{a}_{i,\sigma} + \hat{a}_{i,\sigma}^\dagger) - \psi_\sigma^2) \\
& - zt' \sum_{i,\sigma}^{N_c} (\eta_\sigma (\hat{a}_{i,\sigma}^\dagger + \hat{a}_{i,\sigma}) + \psi_\sigma \hat{a}_{i,\sigma}^\dagger \hat{n}_{i,\sigma} + \psi_\sigma \hat{n}_{i,\sigma} \hat{a}_{i,\sigma} - 2\psi_\sigma \eta_\sigma)
\end{aligned} \tag{2.13}$$

where  $z$  denotes the number of nearest neighbours to site  $i$  that belong to neighbouring clusters.

The energy scale is set by choosing  $t = 1$ , due to which all the physical parameters are considered dimensionless. This cluster Hamiltonian is solved iteratively for  $\psi_\sigma$  and  $\eta_\sigma$  using the self-consistency method as follows:

Beginning with an initial guess for  $\psi_{i,\sigma}$  and  $\eta_{i,\sigma}$ , the Hamiltonian matrix is constructed in the Fock basis  $|\{N_{1,\sigma}\}, \{N_{2,\sigma}\}, \dots, \{N_{C,\sigma}\}\rangle$ . Here  $|\{N_i\}\rangle \equiv |N_{i,1}, N_{i,0}, N_{i,-1}\rangle$  with maximum number of bosons  $N_{max}$  allowed to occupy a lattice site in the cluster. The constructed Hamiltonian is then diagonalized to obtain the ground state energy and eigenvector given by  $|\Psi_{GS}\rangle = \sum_{N_1, N_2, \dots, N_C}^{N_{max}} C_{N_1, N_2, \dots, N_C} |N_{i,1}, N_{i,0}, N_{i,-1}\rangle$ . Using the ground state obtained after diagonalizing, the order parameters  $\psi_{i,\sigma}$  and  $\eta_{i,\sigma}$  are calculated. This process is repeated until the values of  $\psi_{i,\sigma}$  and  $\eta_{i,\sigma}$  are converged and self-consistency condition is fulfilled.

Since the lattice is homogeneous, the order parameters  $\psi_{i,\sigma}$  and  $\eta_{i,\sigma}$  are independent of lattice sites, that is,  $\psi_{i,\sigma} \equiv \psi_\sigma$  and  $\eta_{i,\sigma} \equiv \eta_\sigma$ .

The superfluid density,  $\rho_S$  and boson density,  $\rho$  are calculated using the self-consistent ground state eigenvector as previously discussed in Section 2.2 as  $\rho_S = \sum_\sigma |\psi_\sigma|^2$  and  $\rho = \sum_\sigma \langle \hat{n}_\sigma \rangle$ .

In order to study the magnetic properties of different phases of the Spin-1 Bose Hubbard model, the local magnetic moment identifier  $\langle \vec{F}_i^2 \rangle = \langle (F_i^x)^2 + (F_i^y)^2 + (F_i^z)^2 \rangle$  at a site  $i$  and the global magnetic moment identifier  $\langle F_{TOT}^2 \rangle = \langle (\sum_i^{N_C} \vec{F}_i)^2 \rangle$  are calculated. The nematic order is characterized by the order parameter defined as  $Q_i^{\alpha,\alpha} = \langle F_i^\alpha F_i^\alpha - \frac{1}{3} \vec{F}_i^2 \rangle$  where  $\alpha = x, y, z$ . If  $Q_i^{\alpha,\alpha} = 0$  for all  $\alpha$ , the spins are isotropic, i.e. the spins do not have a preferred direction and behave the same way regardless of orientation. Conversely, spin anisotropy which is characteristic of the nematic order is specified by  $Q_i^{\alpha,\alpha} \neq 0$ . For a positive spin-dependent interaction  $U_2$ , the singlet pair density is given by  $\rho_{SD} = \langle \hat{A}_{SD}^\dagger \hat{A}_{SD} \rangle$  where the singlet creation operator  $\hat{A}_{SD}^\dagger = \frac{1}{\sqrt{6}}(2\hat{a}_1^\dagger \hat{a}_{-1}^\dagger - \hat{a}_0^\dagger \hat{a}_0^\dagger)$ . Homogeneity of the lattice ensures that the local magnetic moment ( $\langle \vec{F}_i^2 \rangle$ ), the nematic order parameter ( $Q_i^{\alpha,\alpha}$ ) and the singlet pair density ( $\rho_{SD}$ ) are site independent.

The present work investigates systems with cluster sizes  $N_C = 1, 2$ .

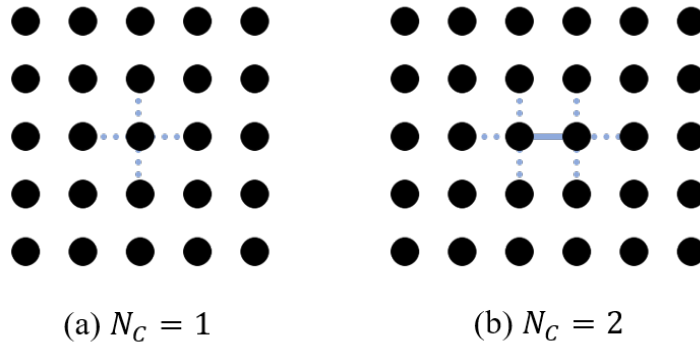


Figure 2.2: Clusters of size (a)  $N_C = 1$  and (a)  $N_C = 2$ . The black dots represent lattice sites and the blue solid line represents intra-cluster hopping. The blue dotted lines depict inter-cluster hopping approximated using mean-field theory.

Another important tool for characterizing quantum phase transitions is quantum entanglement. In order to obtain a signature of quantum entanglement across the distinct phases exhibited by the model, calculations of bipartite Entanglement Entropy (EE) are employed. In recent experiments, the measurement of Rényi Entanglement Entropy has encouraged the study of bipartite entanglement in a system of bosons trapped in optical lattices. Rényi EE is defined by separating the whole system into two subsystems, say A and B. The  $n^{th}$  order Rényi EE is defined as

$$S_n[A(B)] = \frac{1}{1-n} \log[\text{Tr}(\hat{\rho}_{A(B)}^n)] \quad (2.14)$$

where the reduced density matrix of subsystem  $A(B)$  is expressed as  $\hat{\rho}_{A(B)}^n = \text{Tr}_{B(A)}(\hat{\rho}_{AB})$  and  $\hat{\rho}_{AB}$  is the density matrix of the whole system. If the two subsystems, denoted as  $A$  and  $B$ , are entangled, discarding information about one subsystem will leave the other in a mixed quantum state, rather than a pure quantum state. In the present study, the second order ( $n = 2$ ) Rényi EE is calculated for which equation (2.14) is expressed as  $S_2[A(B)] = -\log[\text{Tr}(\hat{\rho}_{A(B)}^2)]$ .

The intra-cluster interactions and tunnelling are treated exactly in the cluster mean field theory calculations and as such intra-cluster bipartite entanglement is studied for a cluster size of  $N_C = 2$  to ensure both subsystems comprise of a single site. Hence, if subsystem  $A$  is one of the two sites belonging to the cluster, then subsystem  $B$  is the remaining site. Therefore, the reduced density matrix for site  $A$  is  $\hat{\rho}_A = \sum_{N_1, N'_1} (\sum_{N_2} C_{N_1, N_2}^* C_{N'_1, N_2}) |N_1\rangle \langle N'_1|$ . The second-order Rényi EE  $S_2$  is calculated for different parameters in the present study.

## 2.4 Finite temperature formalism

The previous two sections highlighted the zero temperature properties of the Spin-1 Bose Hubbard model with density-induced tunnelling where the phase transitions are driven by quantum fluctuations. However, in experimental set-ups, the temperatures are low but finite ( $10^{-9}$  Kelvin). Consequently, thermal fluctuations exist and contribute to the critical quantum region. Hence, it is interesting to learn the effects of thermal fluctuations along with quantum fluctuations.

### 2.4.1 Mean field theory

In this sub-section, the finite temperature scheme is discussed for single-site mean field theory (MFT). The single-site mean-field Hamiltonian expressed in (2.11) is constructed and diagonalized to obtain the eigenvalues  $E_\alpha$  and eigenvectors  $|\alpha\rangle$ . Utilizing these, the partition function, occupation probabilities and thermal averages are calculated as described below.

The partition function is given by

$$\mathcal{Z} = \sum_{\alpha} e^{-\frac{E_{\alpha}}{k_B T}} \quad (2.15)$$

where  $T$  is the temperature and  $k_B$  is the Boltzmann's constant which is set to 1. The occupational probability of a mean-field state  $|\alpha\rangle$  is calculated as

$$P_\alpha = \frac{e^{-\frac{E_\alpha}{k_B T}}}{\mathcal{Z}} \quad (2.16)$$

The thermal average of an operator at finite temperature is expressed as

$$\langle \hat{O} \rangle = \sum_{\alpha} P_\alpha \langle \alpha | \hat{O} | \alpha \rangle \quad (2.17)$$

The superfluid order parameter and the density-induced tunneling order parameter are calculated and the above equations are solved iteratively until the self-consistent condition is satisfied and the order parameters converge. By doing so, the Free Energy  $\mathcal{F} = -k_B T \ln \mathcal{Z}$  is minimized. The superfluid density, boson density and compressibility  $\kappa = \frac{d\rho}{d\mu}$  are obtained using the self-consistent solution. These three quantities are utilized to study the phases and transitions emerging from the model under study. Superfluid (SF) phase is characterized by finite  $\rho_S$  and  $\kappa$  while the Mott Insulator (MI) phase has vanishing  $\rho_S$  and  $\kappa$ . In the finite temperature regime, another phase arises which is the Normal Bose Liquid (NBL). The NBL phase exhibits vanishing  $\rho_S$  but finite  $\kappa$ . The SF and MI phases transition into the NBL phase as temperature is increased.

### 2.4.2 Cluster Mean Field Theory

The previous sub-section illustrated the finite temperature single-site MFT. Developing upon the former discussion, the CMFT formalism will be extended to finite temperatures in this sub-section.

The cluster mean-field Hamiltonian (2.13) is constructed in the Fock basis of the cluster with an initial guess of  $\psi_\sigma$  and  $\eta_\sigma$ . The Hamiltonian matrix is diagonalized to obtain the eigenvalues  $E_\alpha$  and eigenvectors  $|\alpha\rangle$ . Using these eigenvalues and eigenvectors, the partition function, occupation probabilities and thermal averages are calculated as described below.

The partition function is given by

$$\mathcal{Z} = \sum_{\alpha} e^{-\frac{E_{\alpha}}{k_B T}} \quad (2.18)$$

where  $T$  is the temperature and  $k_B$  is the Boltzmann's constant which is set to 1. The occupation probabilities of each cluster mean-field state  $|\alpha\rangle$  is calculated as

$$P_{\alpha} = \frac{e^{-\frac{E_{\alpha}}{k_B T}}}{\mathcal{Z}} \quad (2.19)$$

The thermal average of an operator at finite temperature is expressed as

$$\langle \hat{O} \rangle = \sum_{\alpha} P_{\alpha} \langle \alpha | \hat{O} | \alpha \rangle \quad (2.20)$$

Using these three quantities, the order parameters  $\psi_{\sigma}$  and  $\eta_{\sigma}$  are calculated and the above procedure is carried out in an iterative manner until self-consistency condition is fulfilled. The scheme described above ensures minimization of Free Energy  $\mathcal{F} = -k_B T \ln \mathcal{Z}$ . The superfluid density  $\rho_S = \sum_{\sigma} |\psi_{\sigma}|^2$ , boson density  $\rho = \sum_{\sigma} \langle \hat{n}_{\sigma} \rangle$  and compressibility  $\kappa = \frac{d\rho}{d\mu}$  are obtained using the self-consistent solution. In addition to these, the local magnetic moment  $\langle \vec{F}^2 \rangle$ , the global magnetic moment  $\langle F_{TOT}^2 \rangle$ , the nematic order parameter  $Q^{\alpha,\alpha}$  for  $\alpha = x, y, z$  and the singlet pair density  $\rho_{SD} = \langle \hat{A}_{SD}^{\dagger} \hat{A}_{SD} \rangle$  where the singlet creation operator  $\hat{A}_{SD}^{\dagger} = \frac{1}{\sqrt{6}}(2\hat{a}_1^{\dagger} \hat{a}_{-1}^{\dagger} - \hat{a}_0^{\dagger} \hat{a}_0^{\dagger})$  are calculated to study the magnetic properties of the different phases that arise in the model. The Superfluid (SF) and Mott Insulator (MI) phases transition to the Normal Bose Liquid (NBL) as temperature is increased. The NBL phase exhibits vanishing  $\rho_S$  but finite  $\kappa$ . The present work investigates systems with cluster sizes  $N_C = 1, 2$ .

# Chapter 3

## Results

The Spin-1 Bose Hubbard Model with density-induced tunnelling has been studied for the case  $U_2 > 0$ . The results are ordered in both the sections as follows: Spin-1 BHM without DIT, Spin-1 BHM at finite temperature, Spin-1 BHM with DIT, and lastly, Spin-1 BHM at finite temperature with DIT.

### 3.1 2D: Single Site

In the case of  $U_2 > 0$  the superfluid (SF) phase has  $\frac{U(1) \times S^2}{Z_2}$  symmetry [37]. This is called polar superfluid (PSF). The superfluid order parameters  $\psi_\sigma$  are considered to be real. Hence, taking the symmetry into account, the order parameters can have two possible set of values:  $\psi_1 = \psi_{-1} \neq 0$  and  $\psi_0 = 0$  or  $\psi_1 = \psi_{-1} = 0$  and  $\psi_0 \neq 0$  [37].

In order to study the phases arising in the system, the order parameters and densities are plotted against chemical potential  $\mu$  in figure 3.1 for on-site interaction  $U_0 = 24.0$  and  $U_2/U_0 = 0.03$ . From the plot of superfluid order parameters against chemical potential  $\mu$ , it is observed that the polar symmetry is conserved and superfluidity contribution comes from  $\sigma = \pm 1$  bosons.

The superfluid order parameters  $\psi_{\pm 1}$  are finite in the superfluid phase as opposed to the MI phase where  $\psi_{0,\pm 1} = 0$ . The superfluid density and total density plots show the transition from the SF phase (where  $\rho_S \neq 0$ ) to the MI phase (where  $\rho_S = 0$  and  $\rho = 1, 2$ ).

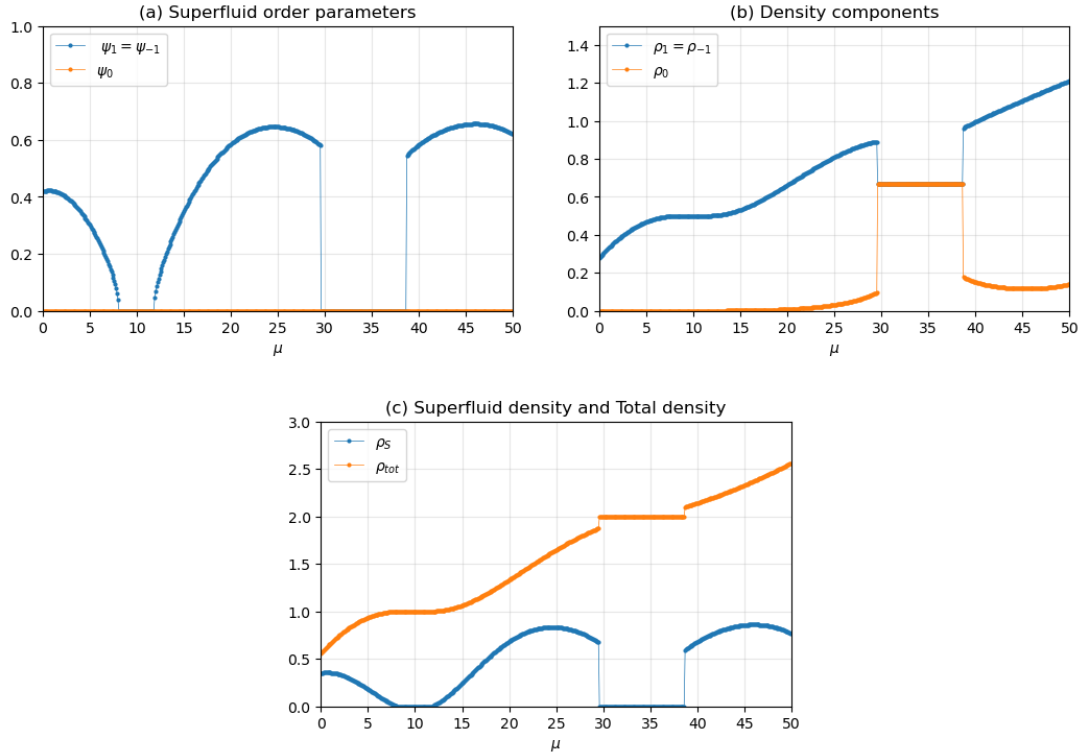


Figure 3.1: Plots of (a) superfluid order parameters  $\psi_\sigma$ , (b) individual density components  $\rho_\sigma$  and (c) superfluid density  $\rho_S$  and total density  $\rho_{tot}$  versus the chemical potential  $\mu$  for  $U_2/U_0 = 0.03$  where  $U_0 = 24.0$  and density-induced tunnelling strength  $t' = 0$ .

To understand the nature of these phase transitions, the ground state energy  $E_0$  is plotted in figure 3.2 as a function of superfluid order parameter  $\psi_{\pm 1}$  near the SF-MI transition for Mott lobes corresponding to density  $\rho = 1, 2$ . Since  $\psi_0 = 0$ , the ground state energy is a function of  $\psi_1 = \psi_{-1}$ .

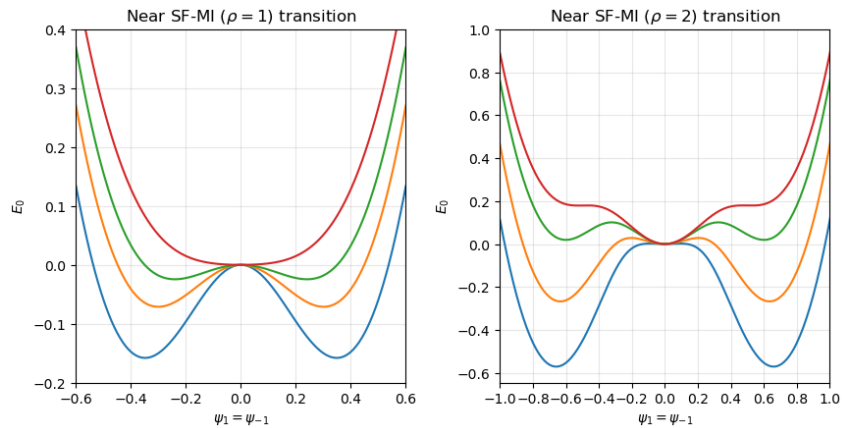


Figure 3.2: Ground state energies  $E_0$  against superfluid order parameters  $\psi_1 = \psi_{-1}$ ,  $\psi_0 = 0$  for 2D single-site ( $N_C = 1$ ) near SF-MI transition (a)  $\rho = 1$  and (b)  $\rho = 2$  for  $U_2/U_0 = 0.03$  where  $U_0 = 24.0$  and density-induced tunnelling strength  $t' = 0$ . Chemical potential  $\mu$  increases from the blue to the red line across the phase transition.

From these plots, it is visible that the phase transition from SF to  $\rho = 1$  MI is continuous whereas a first order transition is seen from SF to  $\rho = 2$  MI. This first order nature arises due to singlet formation in the  $\rho = 2$  MI. The density distribution for  $\rho = 1$  MI indicates that the system is composed of bosons having  $\sigma = \pm 1$  components. In the  $\rho = 2$  MI state, the density distribution is centered around  $2/3$ , that is,  $\rho_1 = \rho_0 = \rho_{-1} = 2/3$ . The existence of a small but finite  $\rho_0$  in the polar SF implies that bosons having spin component  $\sigma = 0$  are in the NBL state.

The phase diagram plot of chemical potential  $\mu$  versus on-site interaction  $U_0$  for 2D single site is plotted in figure 3.3.

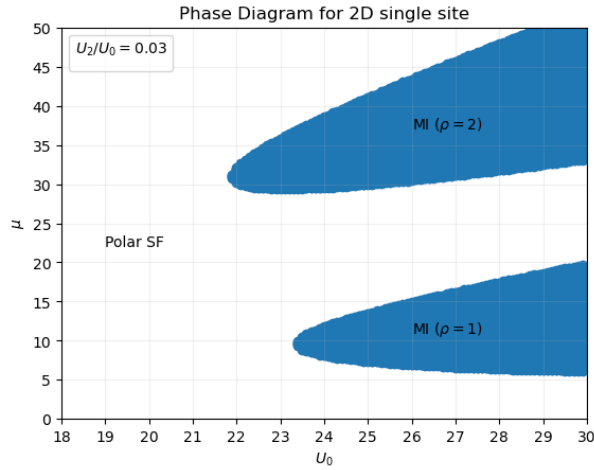


Figure 3.3: Phase diagram plot for 2D single site without density-induced tunneling ( $t' = 0$ ) for  $U_2/U_0 = 0.03$ .

It is seen that for  $U_2 > 0$  the MI phase corresponding to density  $\rho = 2$  is stable over a wider region of parameter space. This can be understood as follows: In the  $\rho = 2$  MI phase, the number of bosons occupying a site are exactly two, allowing a total spin of either  $S = 0$  or  $S = 2$  at every site. An energy difference comes about due to the low-energy singlet  $S = 0$  and  $S = 2$  states since the spin-dependent interaction  $U_2 > 0$ . The transition from the MI to the SF phase requires an energy of  $\sim U_2$  to break this favoured singlet state. This gives a rough estimate for the latent heat of the first-order transition noted above if  $0 \lesssim T$ . This energy barrier makes MI phases with even densities more stable than those with odd densities, thereby explaining the larger  $\rho = 2$  lobe in figure 3.3 as compared to the  $\rho = 1$  lobe.

### 3.1.1 Finite temperature

The previous section discussed the phases and transitions occurring in a 2D single site spin-1 model at zero temperature. Expanding on these, the spin-1 BHM shall be studied at finite temperature in this section.

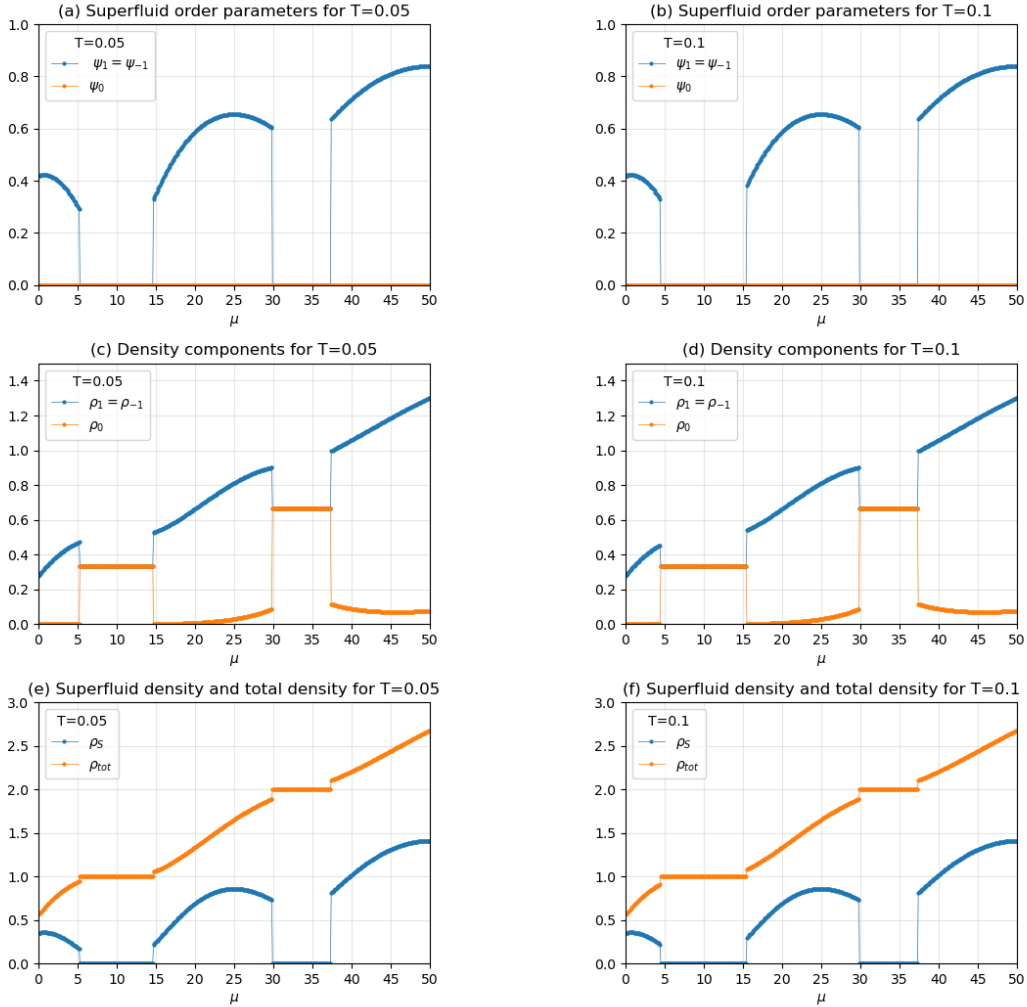


Figure 3.4: Comparison plots of superfluid order parameters, individual density components and superfluid and total density versus the chemical potential  $\mu$  for temperature  $T = 0.05$  and  $T = 0.1$  for  $U_2/U_0 = 0.03$  where  $U_0 = 24.0$  and density-induced tunnelling strength  $t' = 0$ .

At temperature  $T = 0$ , the polar nature of the superfluid phase is portrayed through the superfluid order parameters which take up values  $\psi_1 = \psi_{-1} \neq 0$  and  $\psi_0 = 0$ . This nature persists even at finite temperatures as seen in figure (3.4). In order to compare the zero temperature and finite temperature results, the graphs in figure 3.4 are plotted for  $U_0 = 24.0$  and  $U_2/U_0 = 0.03$ .

The superfluid order parameters  $\psi_{\pm 1}$  show a discontinuous transition from SF-MI phases. The boson densities in MI ( $\rho = 1$ ) phase are different than the zero temperature case. Here, the  $\rho_0$  component also contributes to the MI phase. The densities of each component are thus  $\rho_1 = \rho_0 = \rho_{-1} = 1/3$ . Whereas in the  $\rho = 2$  MI phase, the density distribution is centered around  $2/3$ , that is,  $\rho_1 = \rho_0 = \rho_{-1} = 2/3$  as seen in the zero temperature case.

The superfluid density and total density plots show the transition from the SF phase (where  $\rho_S \neq 0$ ) to the MI phase (where  $\rho_S = 0$  and  $\rho = 1, 2$ ). The superfluid nature of bosons decreases at finite temperatures since the coherent flow is disrupted due to thermal fluctuations in the system. Since the superfluidity has decreased, the system tends to push into the MI phase. However, as temperature increases, the first order phase transitions become second order.

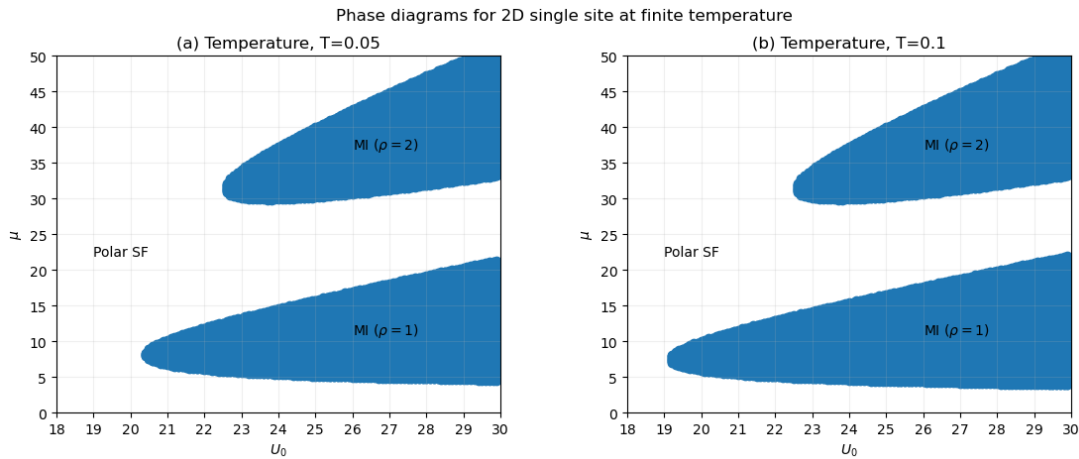


Figure 3.5: Finite temperature phase diagram plots for temperature (a)  $T = 0.05$  and (b)  $T = 0.1$  without density-induced tunneling ( $t' = 0$ ) for  $U_2/U_0 = 0.03$ .

The phase diagram plot of chemical potential  $\mu$  versus on-site interaction  $U_0$  is plotted in figure (3.5) for  $U_2/U_0 = 0.03$  for two different temperatures  $T = 0.05$  and  $T = 0.1$ . It is seen that the  $\rho = 1$  MI phase enlarges with temperature whereas the  $\rho = 2$  MI phase is barely affected as temperature increases. Thermal energy excites bosons leading to a higher population of excited states compared to zero temperature. Superfluidity is disrupted since temperature excites the bosons thus breaking the ordered phase and hindering coherent flow. As temperature increases, superfluidity vanishes. At high enough temperatures, the thermally activated bosons hop between lattice sites even when the on-site interaction  $U_0$  is high. This weakens the Mott phase and it melts into the Normal Bose Liquid (NBL).

Phases	Superfluid density $\rho_S$	Compressibility $\kappa$
Polar Superfluid (SF)	finite	finite
Mott Insulator (MI)	0	0
Normal Bose Liquid (NBL)	0	finite

Table 3.1: The superfluid density and compressibility in the different phases of the Spin-1 Bose Hubbard model

To understand the effect of finite temperature on the phases of the model, the chemical potential  $\mu$  is plotted against temperature for  $U_0 = 28.0$  with  $U_2/U_0 = 0.03$  in figure (3.6). Superfluid (SF) phase is characterized by finite superfluid density  $\rho_S$  and compressibility  $\kappa$  while the Mott Insulator (MI) phase has vanishing  $\rho_S$  and  $\kappa$ . The NBL phase exhibits vanishing  $\rho_S$  but finite compressibility  $\kappa$ . The phases are characterized in Table (3.1). The SF and MI phases transition into the NBL phase as temperature is increased. The MI and NBL phases are not distinct and are thus seen as a crossover. Here, the cross-over boundary is marked by  $\kappa = 0.005$ . It should be noted that this crossover boundary is not a strict phase boundary.

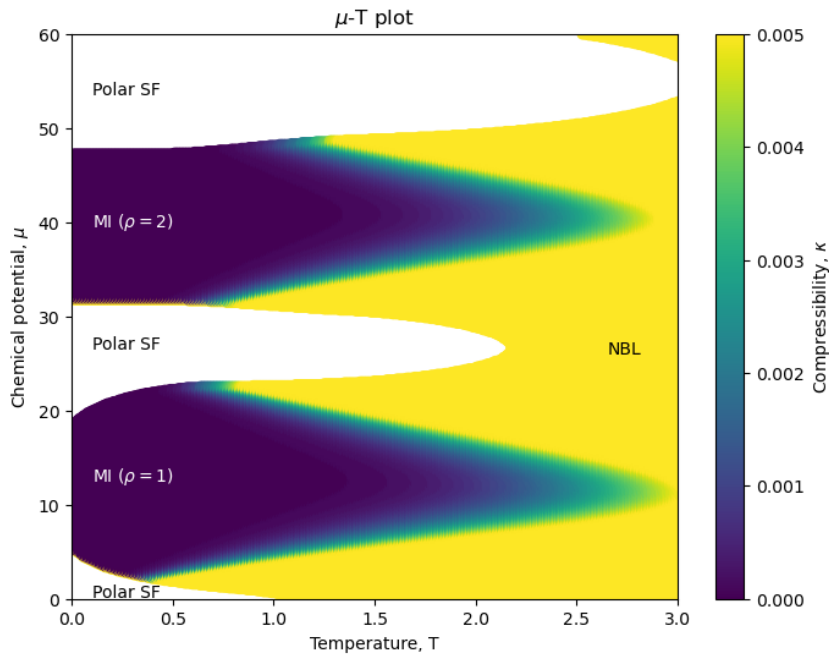


Figure 3.6: Chemical potential  $\mu$  versus temperature  $T$  plot with density-induced tunnelling amplitude  $t' = 0$  for  $U_2/U_0 = 0.03$  and  $U_0 = 28.0$ .

### 3.1.2 Density-Induced Tunnelling

Building upon the investigations of the system's behaviour at zero temperature, this section examines the impact of density-induced tunneling on the Spin-1 BHM.

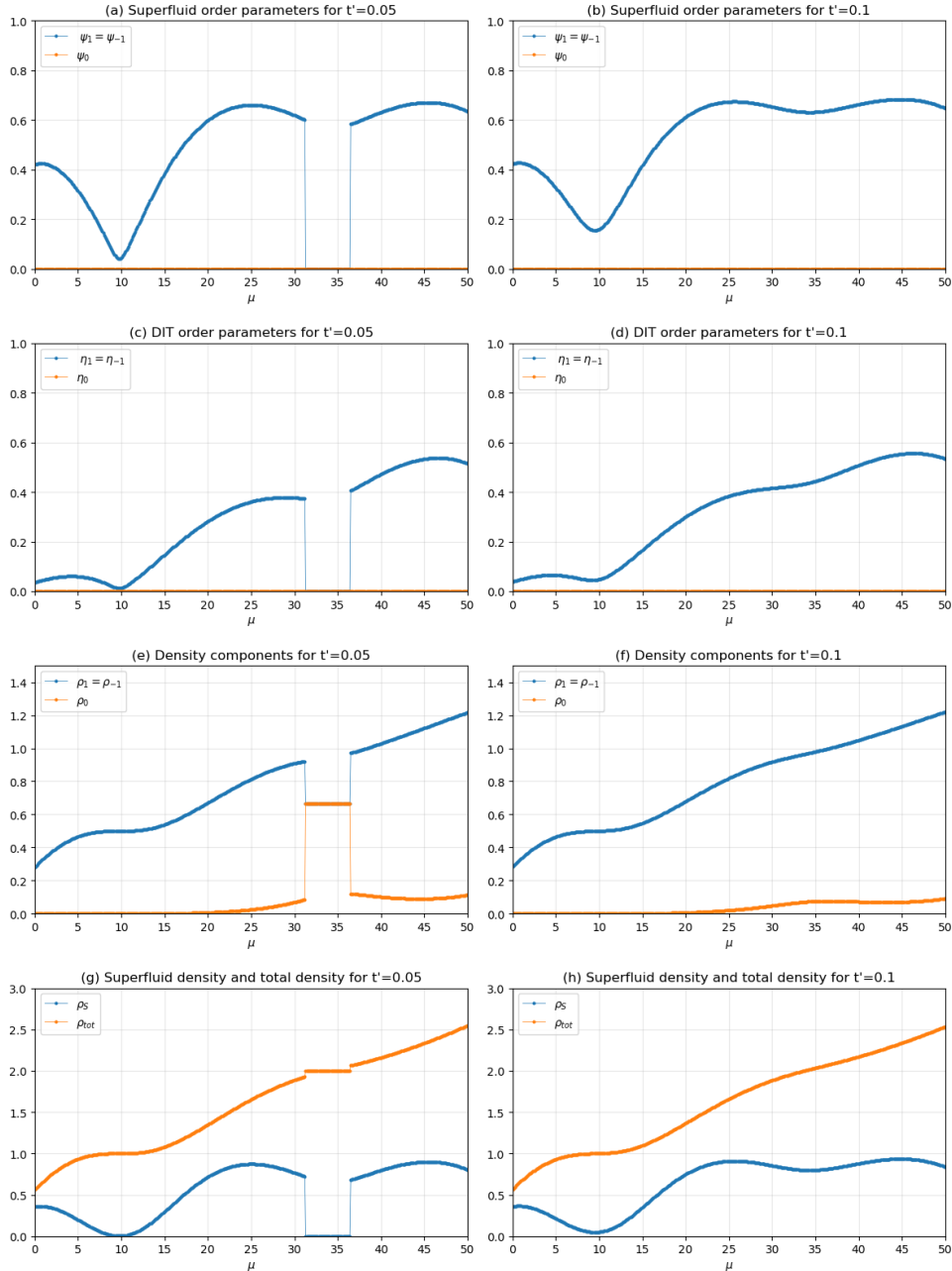


Figure 3.7: Comparison plots of superfluid order parameters  $\psi_\sigma$ , density-induced tunnelling order parameters  $\eta_\sigma$ , boson densities  $\rho_\sigma$  and superfluid density  $\rho_S$  and total density  $\rho_{tot}$  versus the chemical potential  $\mu$  for two different density-induced tunnelling strengths  $t' = 0.05$  and  $t' = 0.1$  for  $U_2/U_0 = 0.03$  where  $U_0 = 24.0$ .

The polar nature of the superfluid phase portrayed through the superfluid order parameters, which take up values  $\psi_1 = \psi_{-1} \neq 0$  and  $\psi_0 = 0$ , persists with the inclusion of density-induced tunnelling. To study the effect of DIT, the graphs in figure 3.7 are plotted for  $U_0 = 24.0$  and  $U_2/U_0 = 0.03$  for different DIT amplitude  $t'$ . Comparing with figure (3.1), it is seen that the superfluidity has increased as DIT amplitude  $t'$  increases. This behaviour was expected since the main effect of density-induced tunnelling (DIT) is

to enhance superfluidity. The order parameters defining the density-induced tunnelling properties are also plotted in the same figure. Their nature is similar to the superfluid order parameters, that is,  $\eta_1 = \eta_{-1} \neq 0$  and  $\eta_0 = 0$  in the superfluid phase and  $\eta_{0,\pm 1} = 0$  in the MI phase.

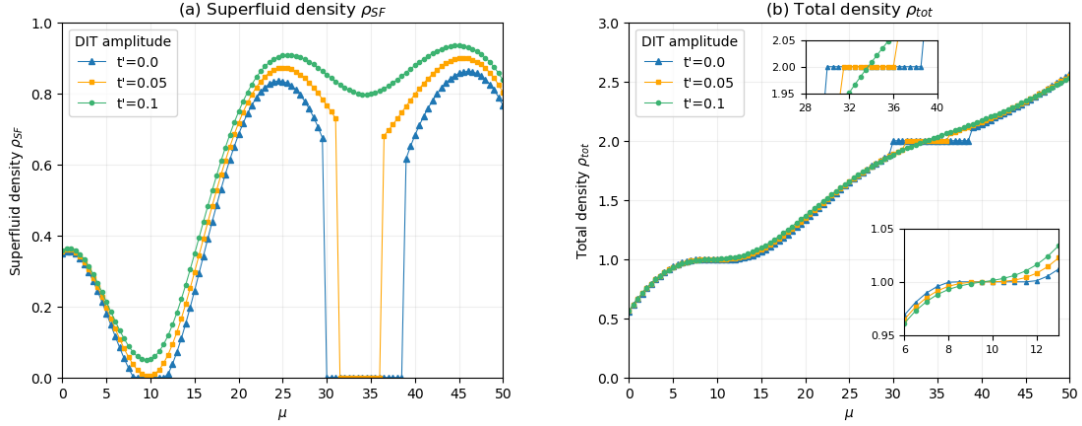


Figure 3.8: Superfluid density  $\rho_S$  and total density  $\rho_{tot}$  plotted against chemical potential  $\mu$  for different density-induced tunnelling amplitudes for  $U_2/U_0 = 0.03$  where  $U_0 = 24.0$ . Insets focus on the MI region for  $\rho = 1, 2$ .

To highlight the effect of density induced tunneling, the superfluid density and total density for  $t' = 0, 0.05$  and  $0.1$  are plotted in figure (3.8). As  $t'$  increases, the Mott Insulator phase diminishes and superfluidity increases. The effect of DIT is seen more prominently at density  $\rho > 1$ .

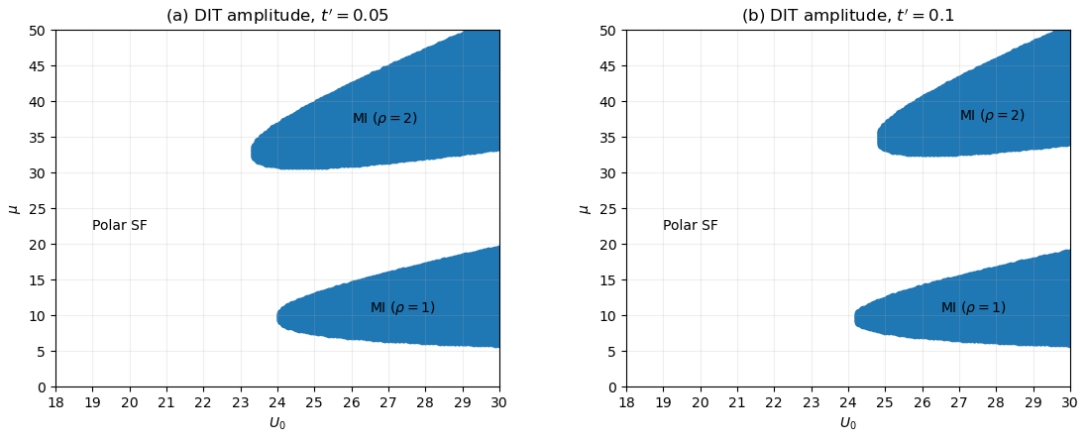


Figure 3.9: Phase diagram plots for density-induced tunnelling amplitude (a)  $t' = 0.05$  and (b)  $t' = 0.1$ .

The phase diagrams with different density-induced tunnelling amplitudes are plotted in figure 3.9 for  $U_2/U_0 = 0.03$ . In contrast to the phase diagram obtained in figure (3.3),

the density-induced tunnelling is seen to have shrunk the MI lobes due to increase in superfluidity. The MI ( $\rho = 2$ ) phase is affected more than the MI ( $\rho = 1$ ) phase.

The effect of DIT amplitude  $t'$  on the critical  $U_0$  can be seen in figure (3.10). It is observed that the density-induced tunnelling results in a shift in the critical  $U_0$  for the SF-MI phase transition. The MI lobe corresponding to density  $\rho = 2$  shifts linearly with an increase in DIT amplitude whereas the MI lobe corresponding to density  $\rho = 1$  shows a sharp linear shift initially with a gradual reduction.

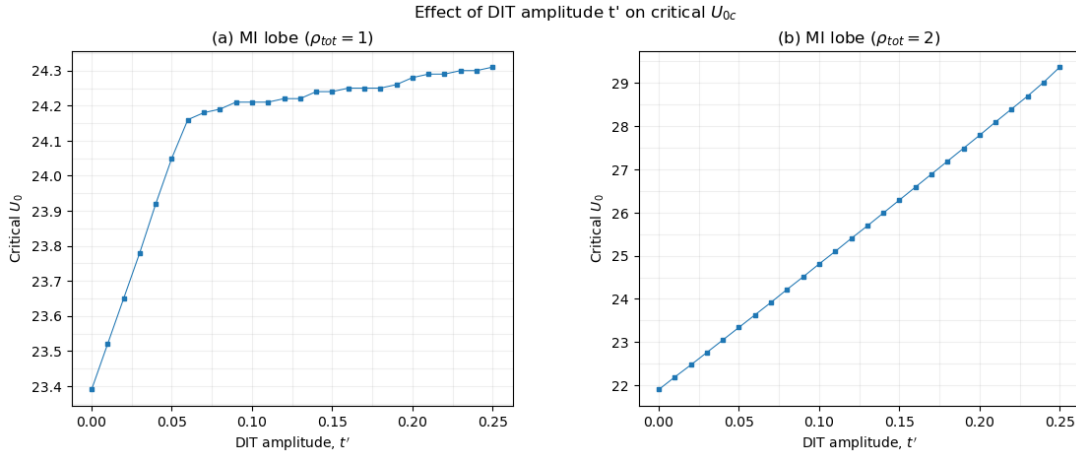


Figure 3.10: Effect of density-induced tunnelling amplitude  $t'$  on the critical  $U_0$  of Mott Insulator phases for  $U_2/U_0 = 0.03$ .

### 3.1.3 Effect of finite temperature on Density-Induced Tunneling

Following the analysis of density-induced tunneling at zero temperature in the previous section, this section examines its effect on the system's properties at finite temperature. To study the effect of DIT and finite temperature on the single-site Spin-1 BHM, the graphs in figure (3.11) and figure (3.12) are plotted for  $U_0 = 24.0$  and  $U_2/U_0 = 0.03$  at different temperatures for DIT amplitude  $t' = 0.05$  and  $t' = 0.1$  respectively.

The plots of superfluid order parameters against chemical potential  $\mu$  reflect the polar nature of the superfluid phase where  $\psi_1 = \psi_{-1} \neq 0$  and  $\psi_0 = 0$ . Analyzing the plots obtained in figure (3.11) and figure (3.12) and comparing them to figure (3.4), it is seen that the density-induced tunnelling affects the Mott Insulator phase by increasing the superfluidity. For the same parameters, the MI ( $\rho = 2$ ) phase vanishes for small DIT amplitude  $t'$  for both temperatures  $T = 0.05$  and  $T = 0.1$ . The density contribution in

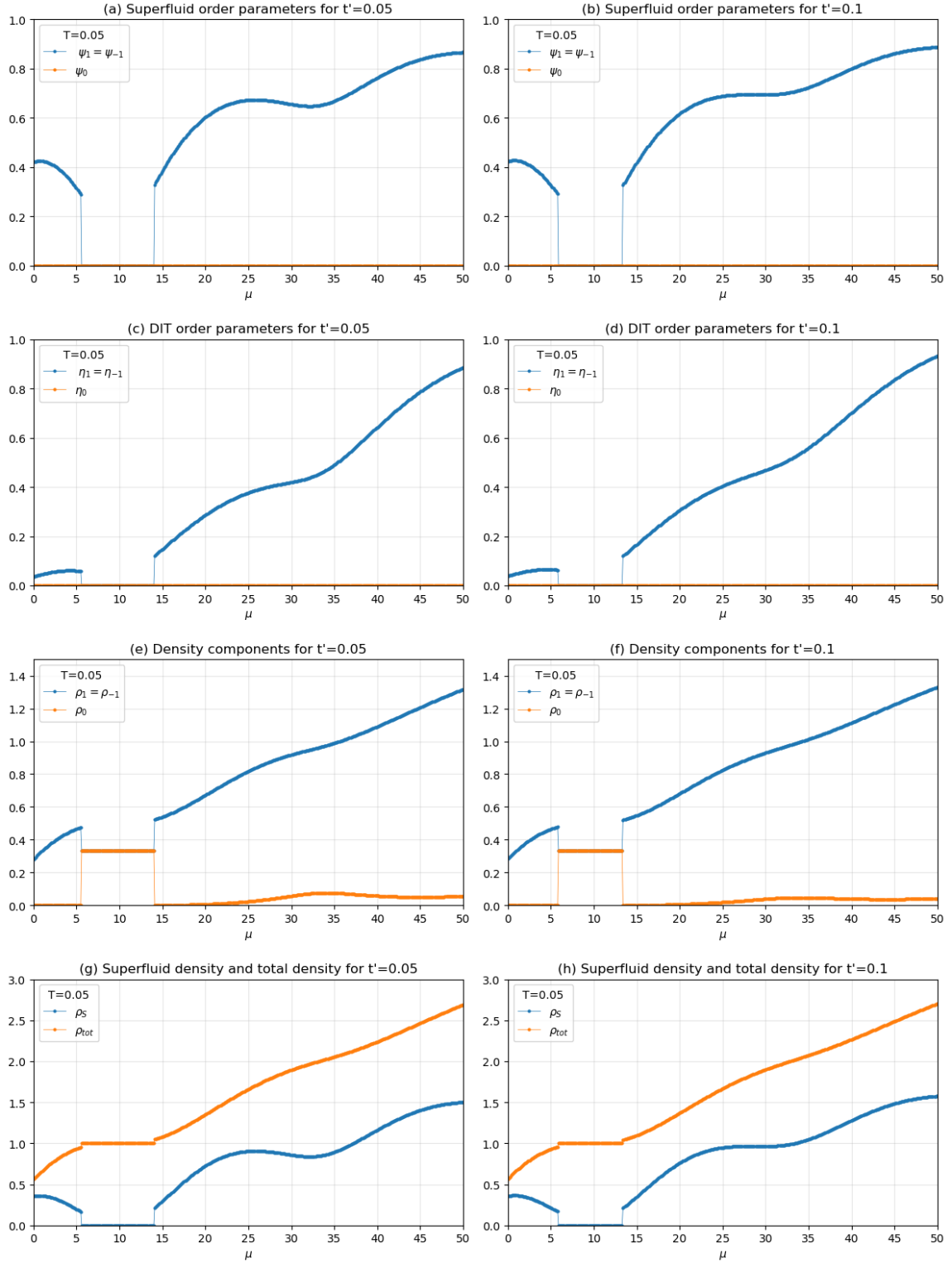


Figure 3.11: Comparison plots of superfluid order parameters  $\psi_\sigma$ , density-induced tunnelling order parameters  $\eta_\sigma$ , boson densities  $\rho_\sigma$  and superfluid density  $\rho_S$  and total density  $\rho_{tot}$  versus the chemical potential  $\mu$  for two different density-induced tunnelling strengths  $t' = 0.05$  and  $t' = 0.1$  at temperature  $T = 0.05$  for  $U_2/U_0 = 0.03$  where  $U_0 = 24.0$ .

MI ( $\rho = 1$ ) phase comes from all three components, that is,  $\rho_1 = \rho_0 = \rho_{-1} = 1/3$ . The

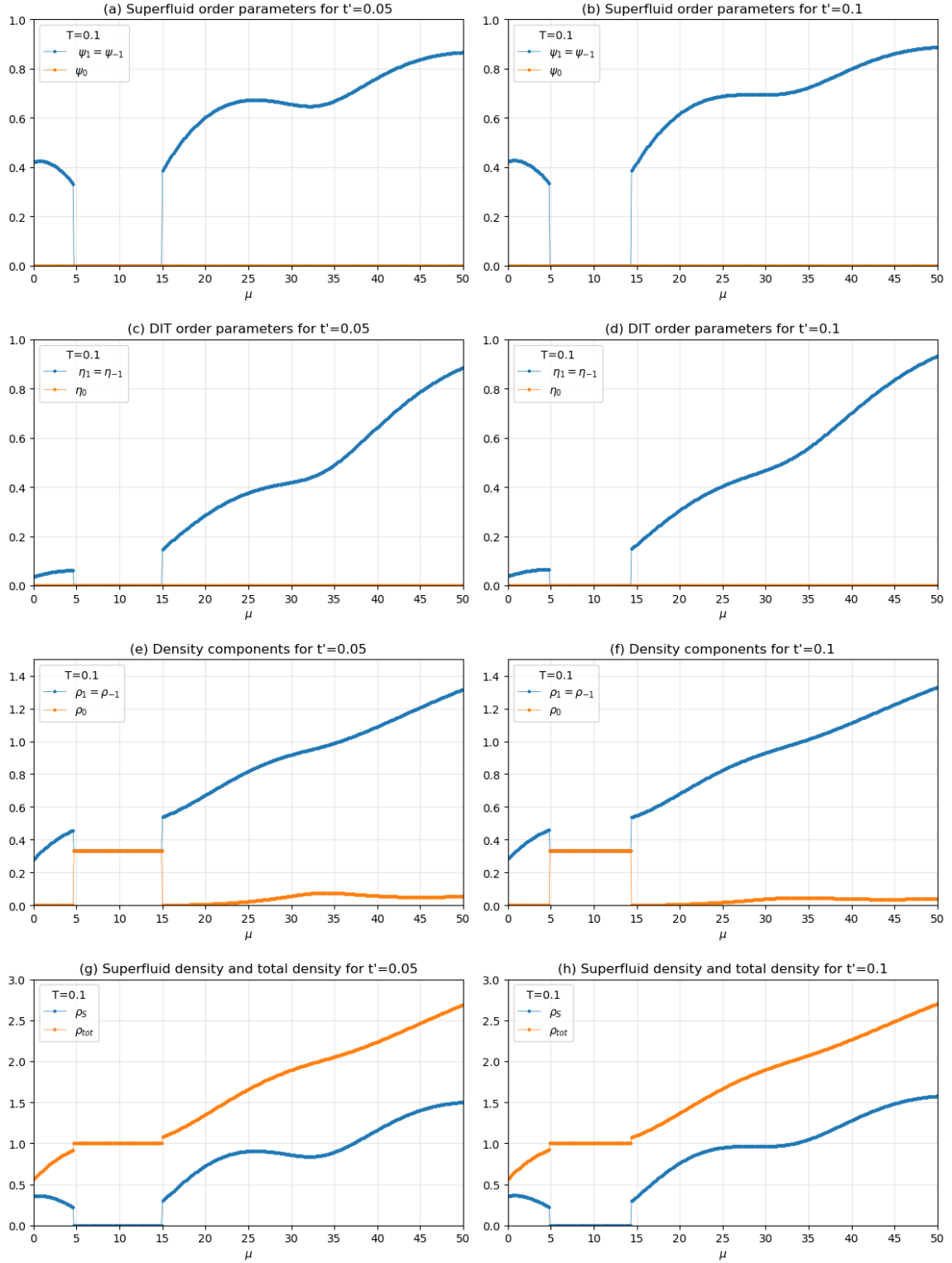


Figure 3.12: Comparison plots of superfluid order parameters  $\psi_\sigma$ , density-induced tunnelling order parameters  $\eta_\sigma$ , boson densities  $\rho_\sigma$  and superfluid density  $\rho_S$  and total density  $\rho_{tot}$  versus the chemical potential  $\mu$  for two different density-induced tunnelling strengths  $t' = 0.05$  and  $t' = 0.1$  at temperature  $T = 0.1$  for  $U_2/U_0 = 0.03$  where  $U_0 = 24.0$ .

superfluid density and total density plots depict the transition from SF phase where  $\rho_S$

is finite to MI phase where  $\rho_S = 0$  and the density is fixed to an integer value at each site. However, at higher temperatures, the MI phase melts into the NBL phase where the compressibility is finite and particle density at a site is not an integer.

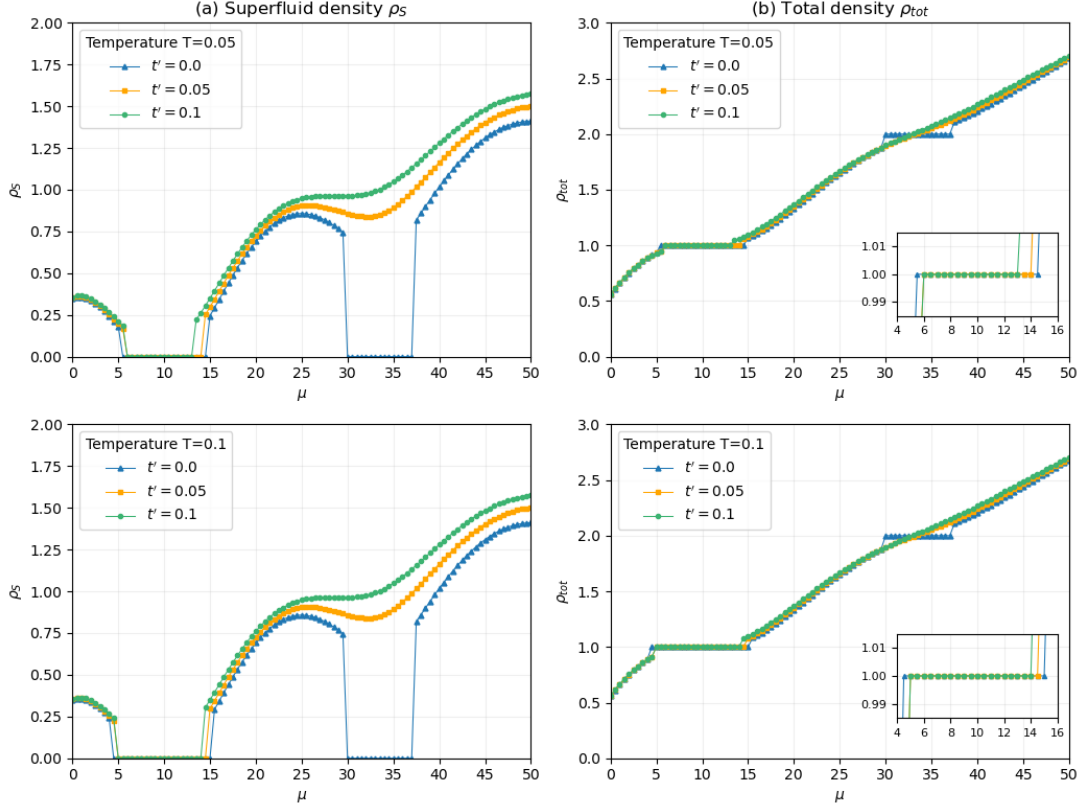


Figure 3.13: Comparison plots of (a) superfluid density  $\rho_S$  and (b) total density  $\rho_{tot}$  versus the chemical potential  $\mu$  for different density-induced tunnelling strengths at temperature  $T = 0.05$  and  $T = 0.1$  for  $U_2/U_0 = 0.03$  where  $U_0 = 24.0$ . Insets highlight the MI ( $\rho = 1$ ) phase for both temperatures  $T = 0.05$  and  $T = 0.1$ .

To gain deeper insights into the influence of density-induced tunneling at finite temperature, the superfluid density and total density are plotted for DIT amplitude  $t' = 0.05$  and  $t' = 0.1$  at two different temperatures in figure (3.34). The density-induced tunneling has affected the MI phase corresponding to density  $\rho = 2$  more prominently. At finite temperature, the superfluidity decreases thus increasing the MI phases. At a particular temperature, as the density-induced tunnelling amplitude increases, the Mott Insulator phase diminishes. Subsequently the superfluidity increases. However, at a given amplitude of density-induced tunnelling, as temperature increases, the Mott insulating phase increases.

The phases arising due to finite temperature and DIT are emphasized in the phase dia-

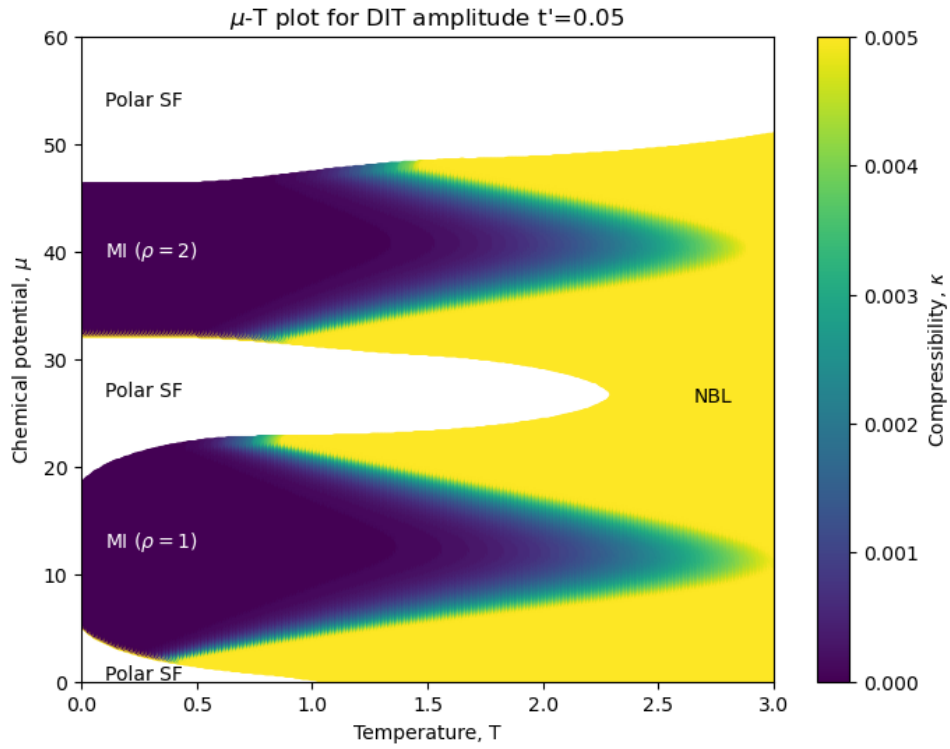


Figure 3.14: Chemical potential  $\mu$  versus temperature  $T$  plot with density-induced tunnelling amplitude  $t' = 0.05$  for  $U_2/U_0 = 0.03$  and  $U_0 = 28.0$ .

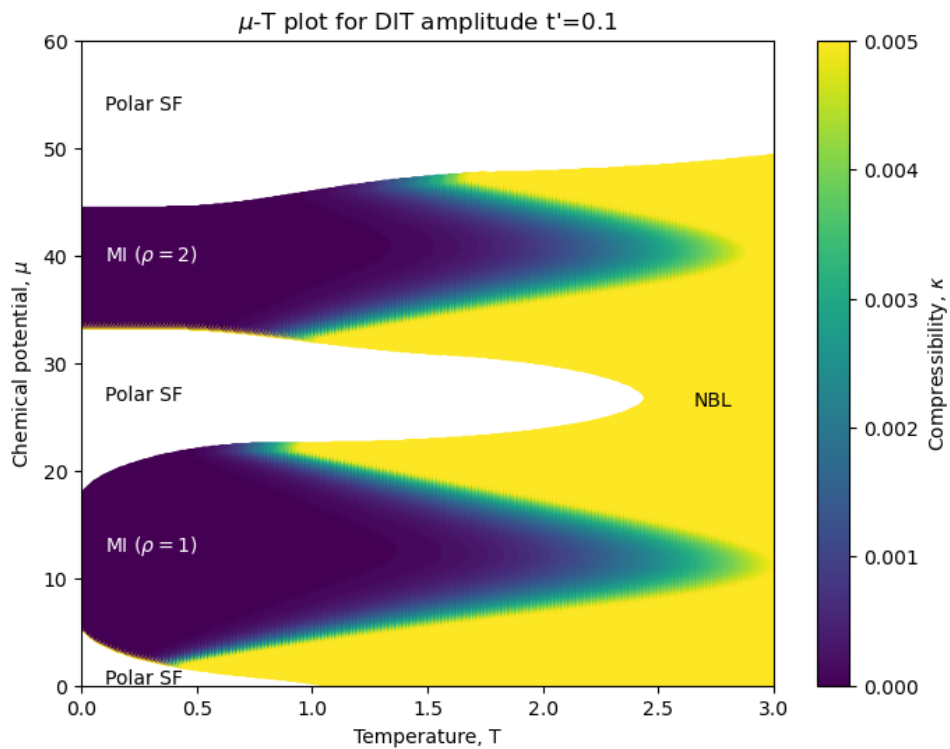


Figure 3.15: Chemical potential  $\mu$  versus temperature  $T$  plot with density-induced tunnelling amplitude  $t' = 0.1$  for  $U_2/U_0 = 0.03$  and  $U_0 = 28.0$ .

grams in the  $\mu - T$  plane plotted for  $U_2/U_0 = 0.03$ . The plots in figure (3.14) and figure (3.15) illustrate the effect of density-induced tunnelling on finite temperatures. The superfluidity is seen to increase across both the phase diagrams and MI phases shrink. The compressibility is not affected by the inclusion of the density-induced tunnelling. The MI-NBL phase is a cross-over and the cross-over boundary is marked by cross-over compressibility  $\kappa = 0.005$ . It should be noted that this crossover boundary is not a strict phase boundary.

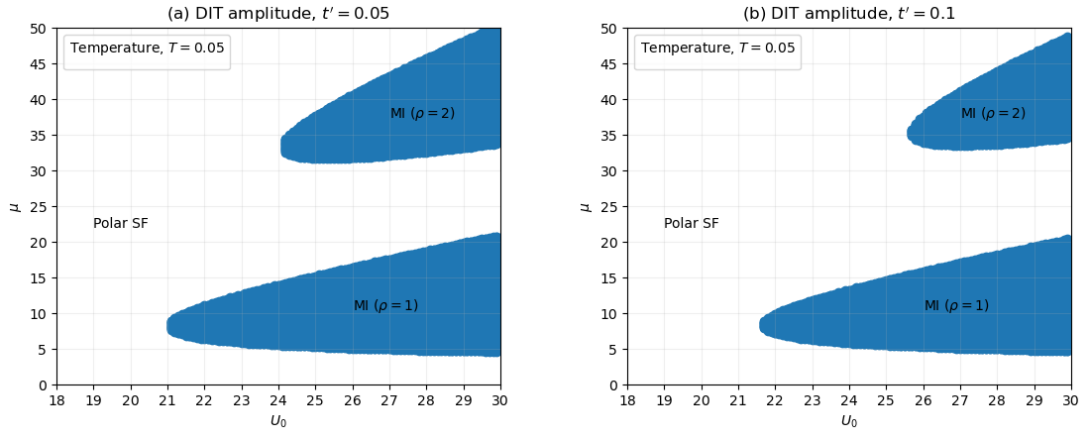


Figure 3.16: Phase diagram plots for  $U_2/U_0 = 0.03$  at temperature  $T = 0.05$  for density-induced tunneling amplitude (a)  $t' = 0.05$  and (b)  $t' = 0.1$ .

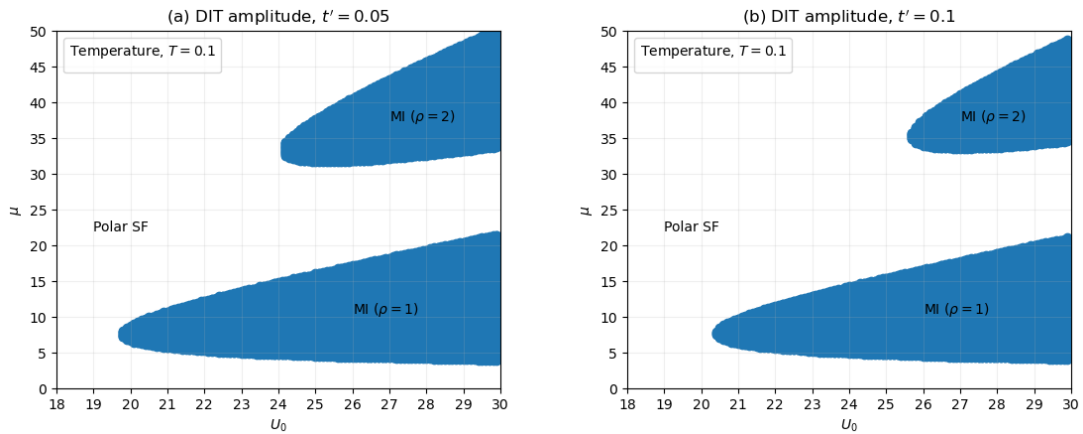


Figure 3.17: Phase diagram plots for  $U_2/U_0 = 0.03$  at temperature  $T = 0.1$  for density-induced tunneling amplitude (a)  $t' = 0.05$  and (b)  $t' = 0.1$ .

The phase diagrams in the  $\mu - U_0$  plane are plotted for density-induced tunneling amplitude (a)  $t' = 0.05$  and (b)  $t' = 0.1$  with  $U_2/U_0 = 0.03$ . The effect of density-induced tunnelling is eminent in both the plots. Figure (3.16) and figure (3.17) show that the MI lobes corresponding to density  $\rho = 2$  have shrunk considerably even at finite temperatures. The MI lobes corresponding to density  $\rho = 1$  also show a similar nature.

The effect of DIT amplitude  $t'$  on the critical  $U_0$  at finite temperatures can be seen in figure (3.18). The density-induced tunnelling results in a shift in the critical  $U_0$  for the SF-MI phase transition. A linear shift is seen for MI corresponding to  $\rho = 1$  and  $\rho = 2$ .

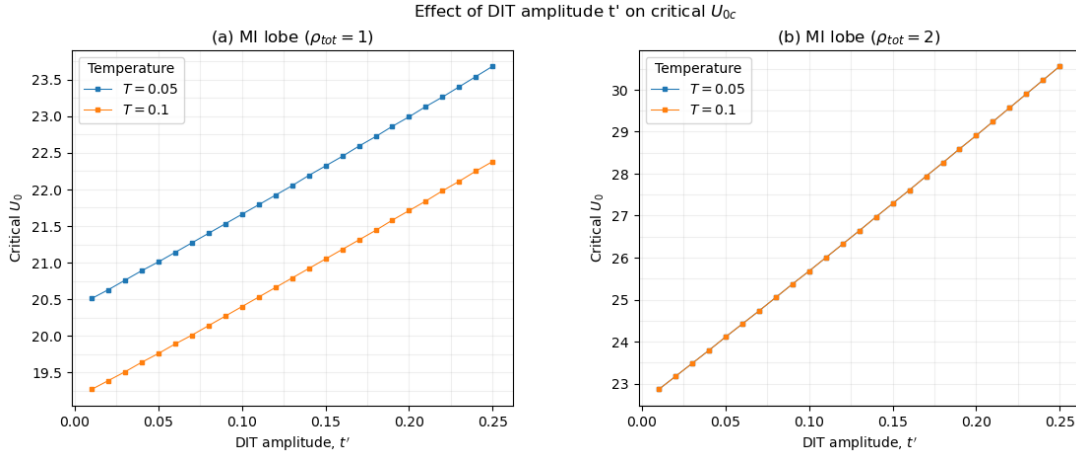


Figure 3.18: Effect of density-induced tunnelling amplitude  $t'$  on the critical  $U_0$  of Mott Insulator phases at finite temperature  $T = 0.05$  and  $T = 0.1$  for  $U_2/U_0 = 0.03$ .

## 3.2 2D: Two site cluster

Single-site spin-1 BHM doesn't fully account for the quantum fluctuations occurring in the system and overestimates the interaction strength required for the SF-MI transition. Therefore, to tackle this, clusters of size  $N_C$  are utilized for a more accurate description of properties. Here, cluster size of  $N_C = 2$  is studied.

The polar nature of the superfluid phase persists and can be seen in the plot of superfluid order parameters against chemical potential  $\mu$  in figure (3.19). As before, the parameters are similar to the previous sections in order to compare the results better, that is,  $U_0 = 24.0$  and  $U_2/U_0 = 0.03$ .

The plots depict that the superfluidity is mainly due to  $\sigma = \pm 1$  components. The densities in MI ( $\rho = 1$ ) phase are centered around  $1/3$ , that is,  $\rho_1 = \rho_{-1} = \rho_0 = 1/3$ . Similarly MI phase corresponding to  $\rho = 2$  is centered around  $2/3$  where each boson having spin-component  $\sigma = -1, 0, 1$  contributes equally to the phase. The superfluid density and total density of bosons describe the phases that come about in the system. The SF-MI phase transitions are discontinuous. The plot of ground state energy as a function of  $\psi_{\pm 1}$  in figure (3.20) shows a discontinuous transition from SF-MI ( $\rho = 2$ ) whereas a small third

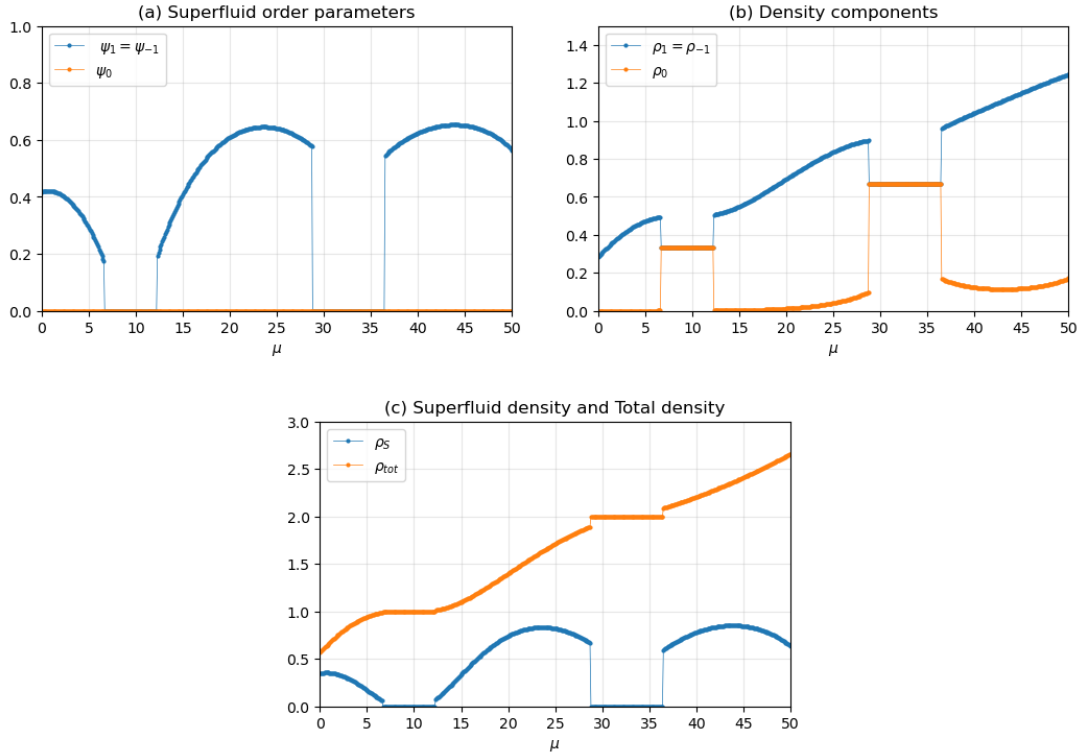


Figure 3.19: Plots of (a) superfluid order parameters  $\psi_\sigma$  (b) individual density components  $\rho_\sigma$  and (c) superfluid density  $\rho_S$  and total density  $\rho_{tot}$  versus the chemical potential  $\mu$  for  $U_2/U_0 = 0.03$  where  $U_0 = 24.0$  and density-induced tunnelling strength  $t' = 0$  for cluster size  $N_C = 2$ .

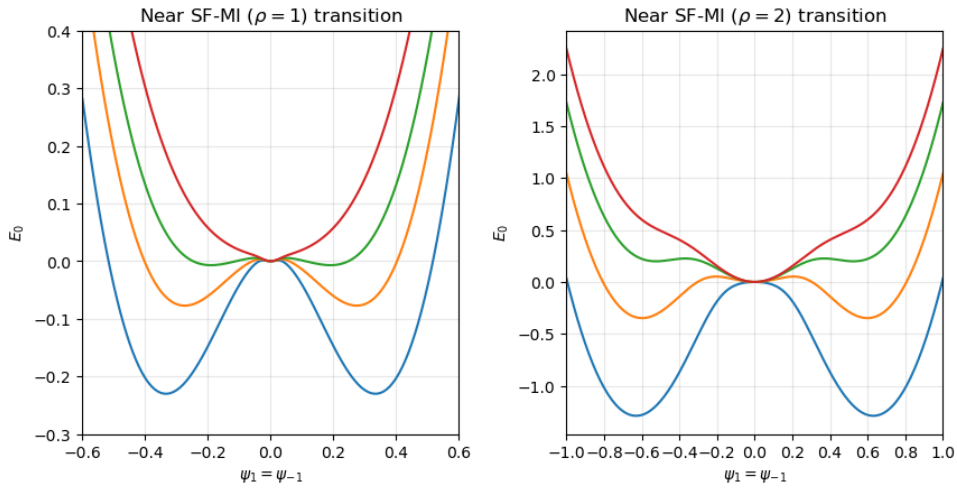


Figure 3.20: Ground state energies  $E_0$  against superfluid order parameters  $\psi_1 = \psi_{-1}$ ,  $\psi_0 = 0$  for 2D two site cluster ( $N_C = 2$ ) near SF-MI transition (a)  $\rho = 1$  and (b)  $\rho = 2$  for  $U_2/U_0 = 0.03$  where  $U_0 = 24.0$ . Chemical potential  $\mu$  increases from the blue to the red line across the phase transition.

minimum representing a weak first order transition is seen from SF-MI ( $\rho = 1$ ). This is in contrast to the two symmetric energy minimas seen in the case of single-site spin-1 BHM

which yield a continuous transition from SF to MI ( $\rho = 1$ ) phase.

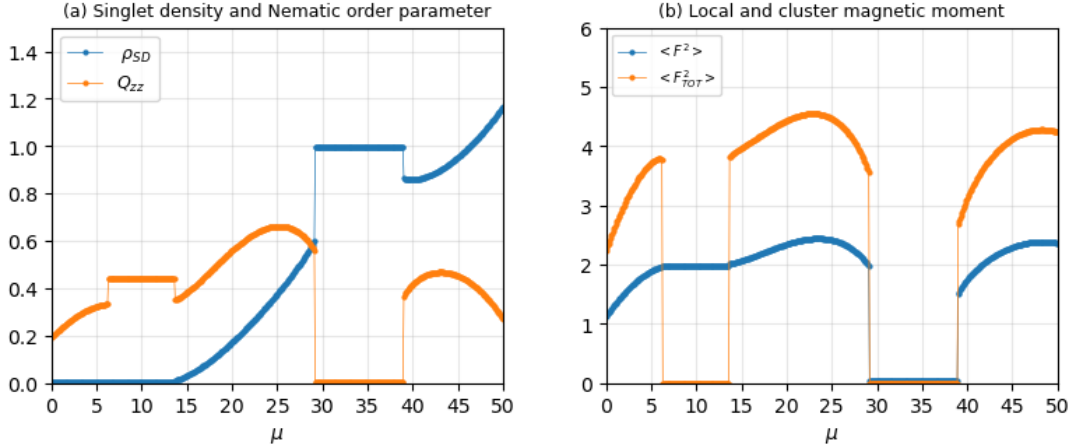


Figure 3.21: Plots of (a) singlet density  $\rho_{SD}$  and nematic order parameter  $Q^{z,z}$  and (b) local magnetic moment  $\langle F^2 \rangle$  and cluster magnetic moment  $\langle F_{TOT}^2 \rangle$  versus the chemical potential  $\mu$  for  $U_2/U_0 = 0.03$  where  $U_0 = 24.0$ .

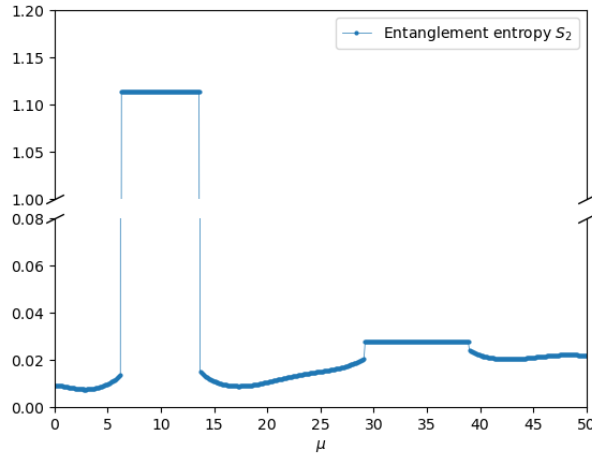


Figure 3.22: Rényi Entanglement Entropy  $S_2$  for  $U_2/U_0 = 0.03$  where  $U_0 = 24.0$ .

The singlet density  $\rho_{SD}$ , nematic order parameter  $Q^{z,z}$ , local magnetic moment  $\langle F^2 \rangle$  and cluster magnetic moment  $\langle F_{TOT}^2 \rangle$  are plotted in figure (3.21). The singlet density  $\rho_{SD}$  is finite when density of bosons  $\rho > 1$  and increases until MI ( $\rho = 2$ ) phase is reached. In the MI ( $\rho = 2$ ) phase, there is one singlet pair at each site and thus singlet density is unity. As the chemical potential  $\mu$  is increased further, the singlet formation reduces due to superfluidity, however, it increases with density  $\rho$ . Nematic order parameter  $Q^{z,z}$  is zero in the  $\rho = 2$  MI phase signifying spin isotropy, and finite everywhere else due to the characteristic nematic phase which shows a preference for a particular spin orientation and breaks the isotropy. The local magnetic moment  $\langle F^2 \rangle = 2$  in the  $\rho = 1$  MI phase since the number of particles at each site is one. However, it is observed that  $\langle F^2 \rangle = 0$

in the MI ( $\rho = 2$ ) phase due to singlet formation. The global (cluster) magnetic moment  $\langle F_{TOT}^2 \rangle = 0$  in the MI phases and is finite in the superfluid phases. Figure (3.22) illustrates the nature of the Rényi EE  $S_2$  as the chemical potential  $\mu$  is varied. From the plot it is observed that the  $\rho = 1$  MI has a larger Rényi EE as compared to the other phases. The CMFT formalism captures the weak quantum tunnelling to nearby sites that occurs in the MI phase even though the bosons are localized at a site. The cluster tends to minimize its total magnetic moment due to the antiferromagnetic interactions at a site. As a result of this, high Rényi EE is recorded since each site is non-locally entangled with the neighbouring sites. The SF-MI phase transition shows a discontinuity in the calculated Rényi EE.

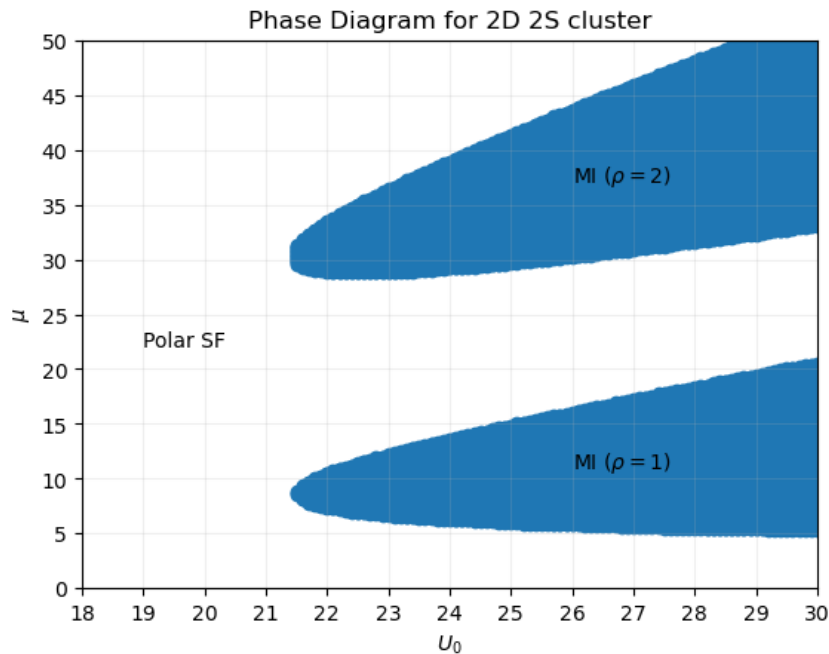


Figure 3.23: Phase diagram plot for 2D two site cluster ( $N_C = 2$ ) without density-induced tunneling ( $t' = 0$ ) for  $U_2/U_0 = 0.03$ .

The phase diagram is plotted in figure (3.23). The critical on-site interaction  $U_0^C$  for phase transition from SF to MI has decreased. Thus, the over-estimation of superfluidity in single-site mean-field calculations has been tackled. This implies that the quantum fluctuations that were neglected in  $N_C = 1$  are accounted for and the system is pushed in the MI phase.

### 3.2.1 Finite temperature

The section above discussed the results of 2D two site cluster at zero temperature. In this section, the results obtained for 2D two sites cluster at finite temperatures shall be discussed.

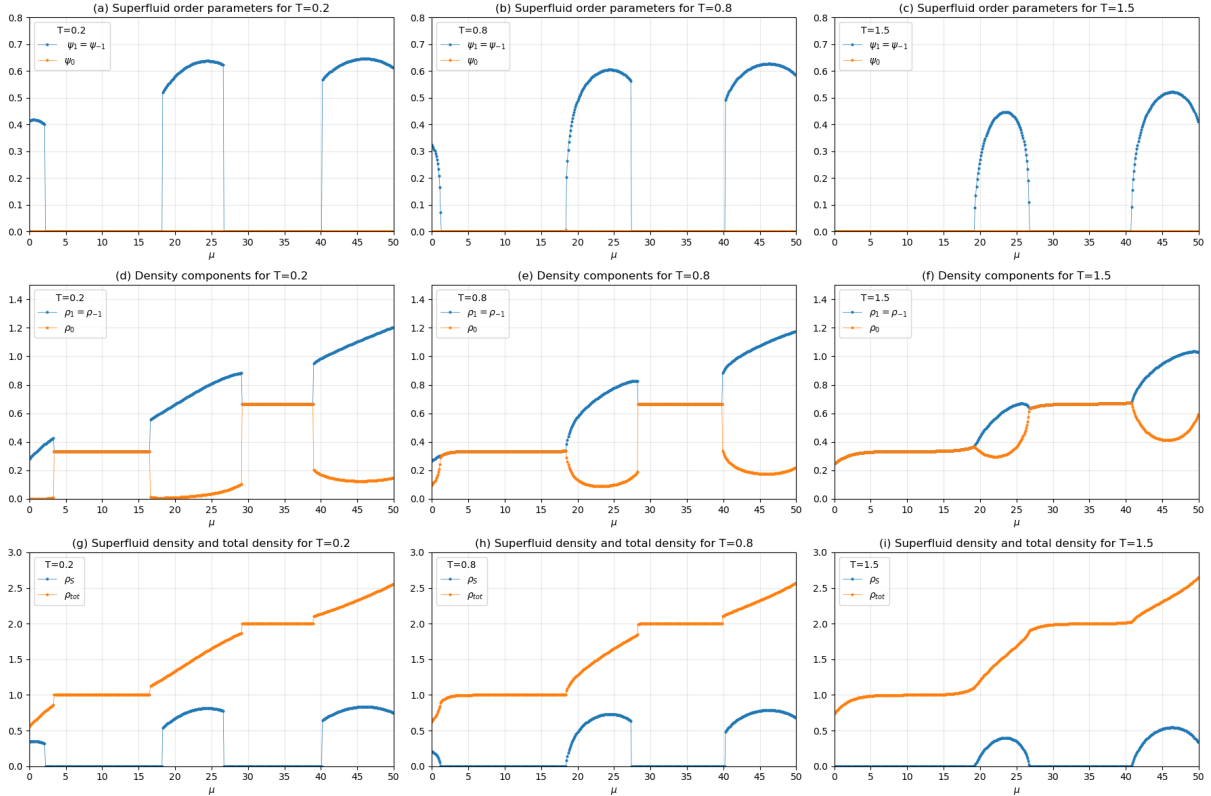


Figure 3.24: Comparison plots of superfluid order parameters  $\psi_\sigma$  individual density components  $\rho_\sigma$  and superfluid density  $\rho_S$  and total density  $\rho_{tot}$  versus the chemical potential  $\mu$  for temperatures  $T = 0.2$ ,  $T = 0.8$  and  $T = 1.5$  for  $U_2/U_0 = 0.03$  where  $U_0 = 24.0$  and density-induced tunnelling strength  $t' = 0$ .

At temperature  $T = 0$ , the polar nature of the superfluid phase is portrayed through the superfluid order parameters which take up values  $\psi_1 = \psi_{-1} \neq 0$  and  $\psi_0 = 0$ . This nature persists even at finite temperatures as seen in figure (3.24). In order to compare the zero temperature and finite temperature results, the graphs in figure 3.24 are plotted for  $U_0 = 24.0$  and  $U_2/U_0 = 0.03$ .

The superfluid order parameters  $\psi_{\pm 1}$  show a discontinuous transition from SF-MI phases. The boson densities in MI ( $\rho = 1$ ) phase are  $\rho_1 = \rho_0 = \rho_{-1} = 1/3$ . Whereas in the  $\rho = 2$  MI phase, the density distribution is centered around  $2/3$ , that is,  $\rho_1 = \rho_0 = \rho_{-1} = 2/3$  as seen in the zero temperature case.

The superfluid density and total density plots show the transition from the SF phase (where  $\rho_S \neq 0$ ) to the MI phase (where  $\rho_S = 0$  and  $\rho_{tot}$  is an integer). With an increase in temperature, the first order phase transitions become second order. This happens since the effect of the spin-dependent interaction term  $U_2$  reduces due to thermal fluctuations in the system. At temperature  $T = 1.5$ , the system shows Normal Bose Liquid (NBL) phase.

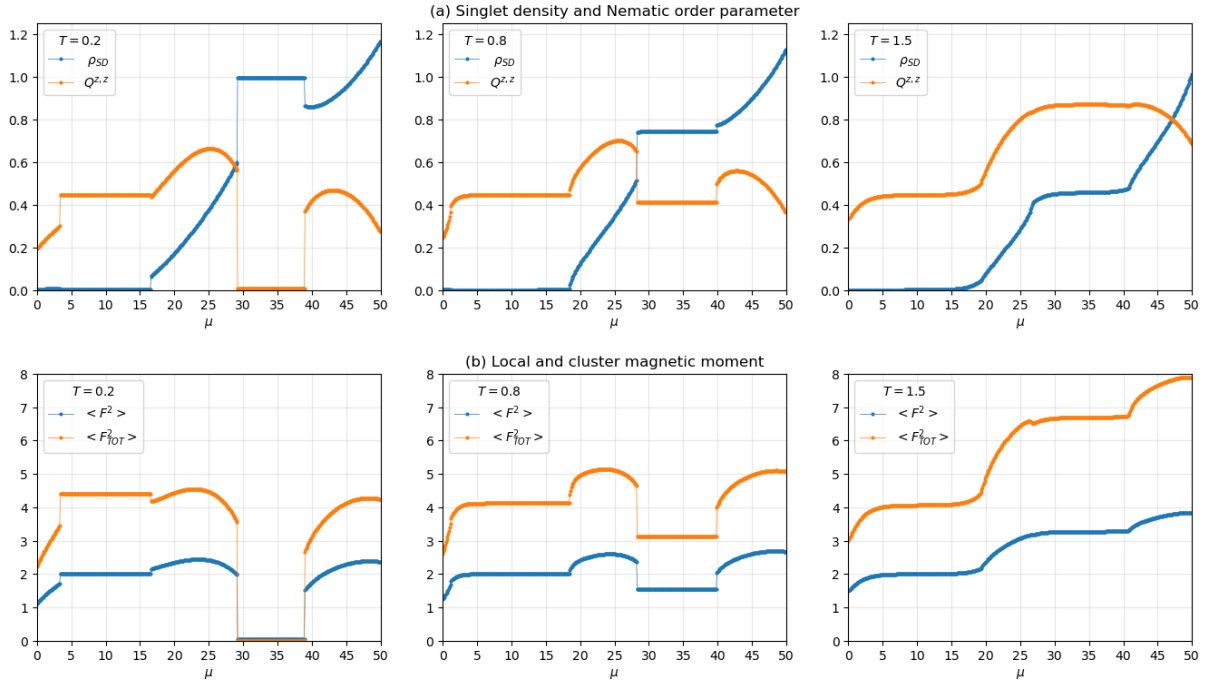


Figure 3.25: Plots of (a) singlet density  $\rho_{SD}$  and nematic order parameter  $Q^{z,z}$  and (b) local magnetic moment  $\langle F^2 \rangle$  and cluster magnetic moment  $\langle F_{TOT}^2 \rangle$  versus the chemical potential  $\mu$  for temperatures  $T = 0.2$ ,  $T = 0.8$  and  $T = 1.5$  for density-induced tunnelling amplitude  $t' = 0$  for  $U_2/U_0 = 0.03$  and  $U_0 = 24.0$ .

The singlet density  $\rho_{SD}$ , nematic order parameter  $Q^{z,z}$ , local magnetic moment  $\langle F^2 \rangle$  and cluster magnetic moment  $\langle F_{TOT}^2 \rangle$  are plotted in figure (3.25) for temperatures  $T = 0.2$ ,  $T = 0.8$  and  $T = 1.5$ . With an increase in temperature, the singlet pairs in the MI ( $\rho = 2$ ) phase start breaking due to thermal fluctuations and thus a decrease in the singlet density is observed. Consequently, the nematic order parameter, local and cluster magnetic moment increase since the antiferromagnetic orientation can be easily broken by small thermal fluctuations. Thereby, the first order nature seen in these plots becomes continuous as temperature increases. These parameters do not show a significant change in the MI ( $\rho = 1$ ) phase.

To understand the phases at finite temperature, the phase diagram in the  $\mu - T$  parameter

space is plotted in figure (3.26 for  $U_0 = 24.0$  and  $U_2/U_0 = 0.03$ . The Mott phase corresponding to  $\rho = 1$  enlarges with temperature since the antiferromagnetic alignment of the spins break in the cluster. This effect is not observed in the MI phase corresponding to  $\rho = 2$  due to singlet formation. The MI-NBL transition is a cross-over and the cross-over boundary is marked by cross-over compressibility  $\kappa = 0.005$ . It should be noted that this crossover boundary is not a strict phase boundary.

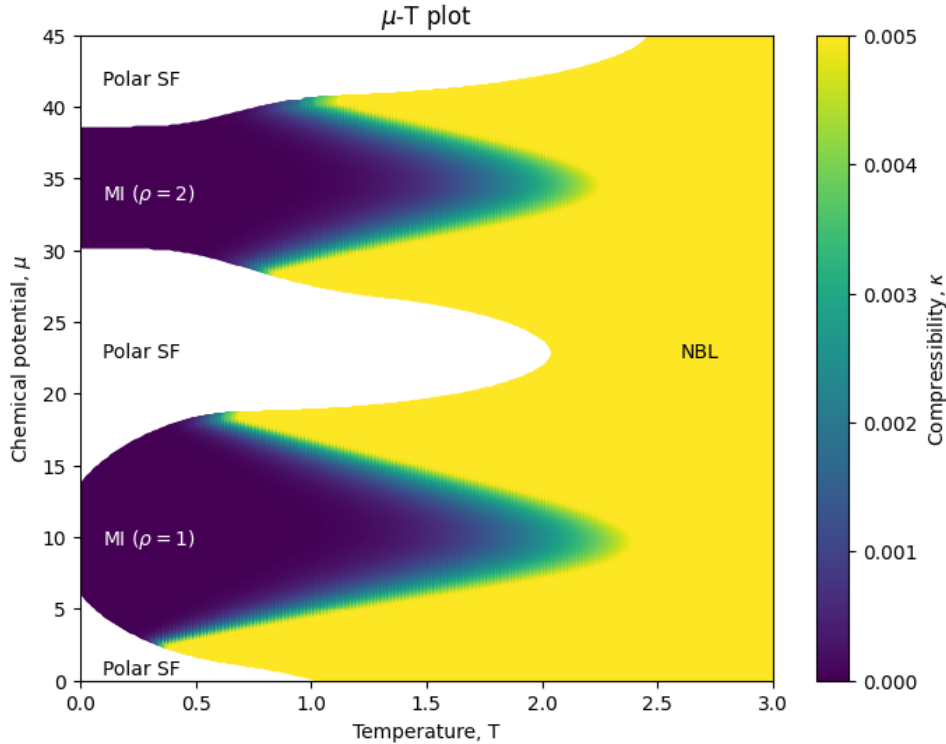


Figure 3.26: Chemical potential  $\mu$  versus temperature  $T$  plot with density-induced tunnelling amplitude  $t' = 0$  for  $U_2/U_0 = 0.03$  and  $U_0 = 24.0$ .

### 3.2.2 Density-Induced Tunneling

Similar to single site spin-1 BHM, the two-site cluster  $N_C = 2$  shall be studied to understand the effect of density-induced tunneling. The density-induced tunneling term describes the tunneling between sites based on the local particle density at those sites.

The plots in figure (3.27) are plotted for the same parameters as the previous two sections for different DIT amplitude  $t'$  so as to analyze and compare the results effectively. The polar nature of the superfluid phase portrayed through the superfluid order parameters, which take up values  $\psi_1 = \psi_{-1} \neq 0$  and  $\psi_0 = 0$ , persists with the inclusion of density-induced tunneling even in the cluster formalism. Comparing with figure (3.19), it is seen

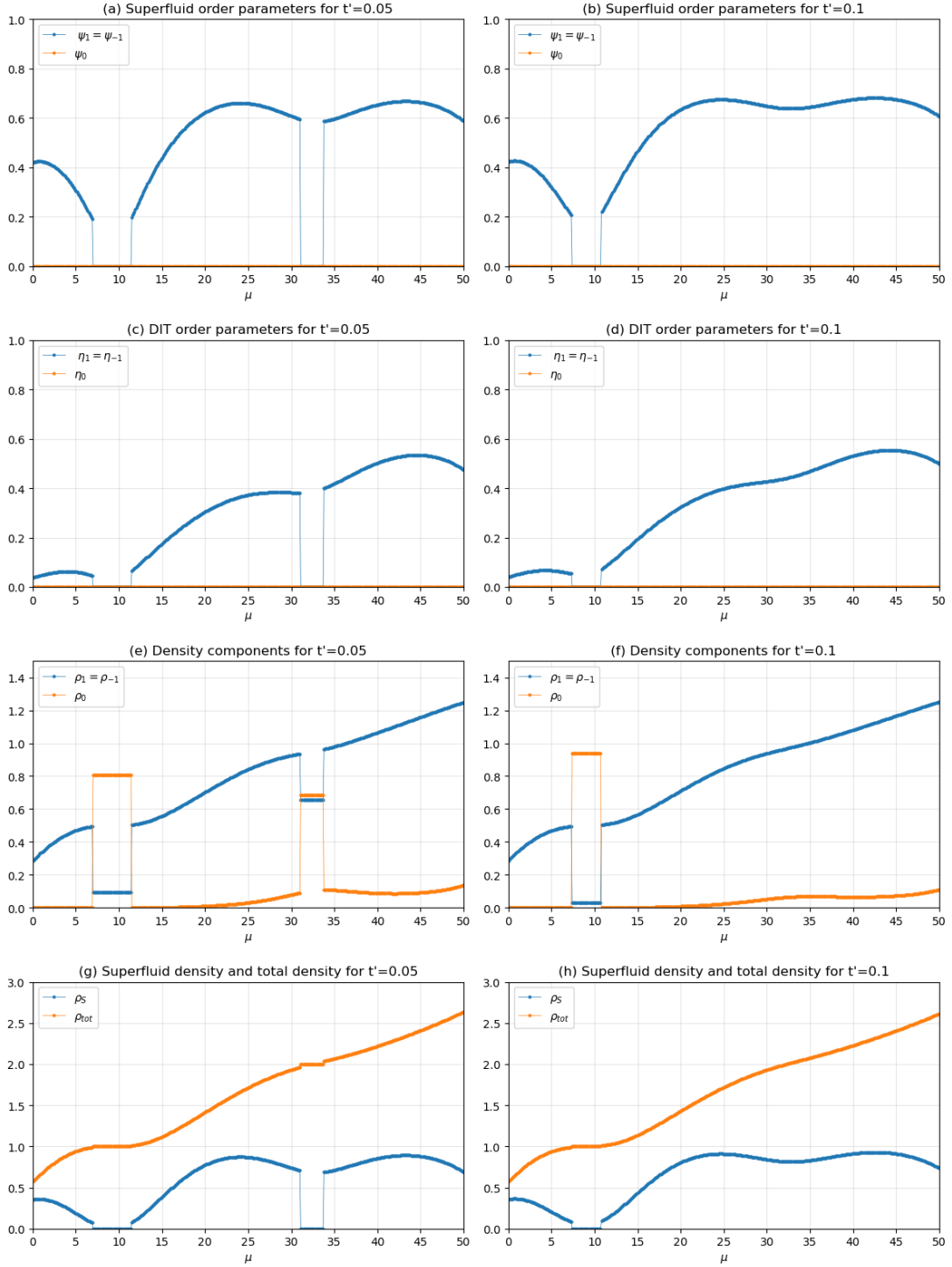


Figure 3.27: Comparison plots of superfluid order parameters  $\psi_\sigma$ , density-induced tunnelling order parameters  $\eta_\sigma$ , boson densities  $\rho_\sigma$  and superfluid density  $\rho_S$  and total density  $\rho_{tot}$  versus the chemical potential  $\mu$  for two different density-induced tunnelling strengths  $t' = 0.05$  and  $t' = 0.1$  for  $U_2/U_0 = 0.03$  where  $U_0 = 24.0$  for cluster size  $N_C = 2$ .

that the superfluidity has increased as DIT amplitude  $t'$  increases. This behaviour is evident in single site as well and is expected since the main effect of density-induced tunnelling (DIT) is to enhance superfluidity.

The density-induced tunneling order parameters follow a similar nature like superfluid order parameters:  $\eta_1 = \eta_{-1} \neq 0$  and  $\eta_0 = 0$  in the superfluid phase and  $\eta_{0,\pm 1} = 0$  in the MI phase. The density distribution in the MI ( $\rho = 1$ ) is slightly different for two site cluster with DIT. The bosons having spin component  $\sigma = \pm 1$  contribute significantly lesser whereas the bosons having spin component  $\sigma = 0$  show higher participation in this phase. The MI ( $\rho = 2$ ) phase also has near equal contribution centered around  $2/3$ . The density distribution attains the equal distribution deep in the MI phase such as for  $U_0 = 40.0$ .

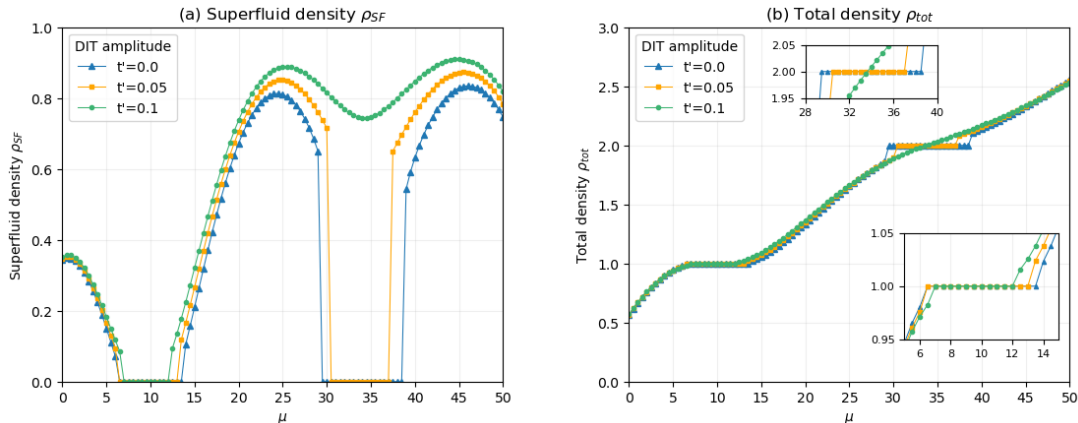


Figure 3.28: (a) Superfluid density  $\rho_S$  and (b) total density  $\rho_{tot}$  plotted against chemical potential  $\mu$  for different density-induced tunnelling amplitudes for  $U_2/U_0 = 0.03$  where  $U_0 = 24.0$ . Insets focus on the MI phase corresponding to  $\rho = 1$  and  $\rho = 2$ .

The plots of superfluid density and total density depict the phases arising in the model. Finite superfluid density indicates that the system is in a superfluid phase whereas superfluid density vanishes when the system is in the Mott Insulator. A comparison between the superfluid densities for different density-induced tunneling amplitudes is done in figure (3.28). Similar comparison is carried out for the total densities for the same set of density-induced tunneling amplitudes. The impact of density-induced tunneling is seen visibly through these plots. As density-induced tunneling amplitude is increased, superfluid behaviour is more strong and the MI phase gets washed out.

The singlet density  $\rho_{SD}$ , nematic order parameter  $Q^{z,z}$ , local magnetic moment  $\langle F^2 \rangle$  and cluster magnetic moment  $\langle F_{TOT}^2 \rangle$  and Rényi EE  $S_2$  are plotted in figure (3.29) for different density-induced tunnelling amplitudes  $t'$ . The singlet density  $\rho_{SD} = 1$  in the MI ( $\rho = 2$ ) phase, however, at higher DIT amplitudes, due to increase in superfluidity the  $\rho = 2$  MI phase vanishes and the singlet density is seen to increase. Consequently, an increase in

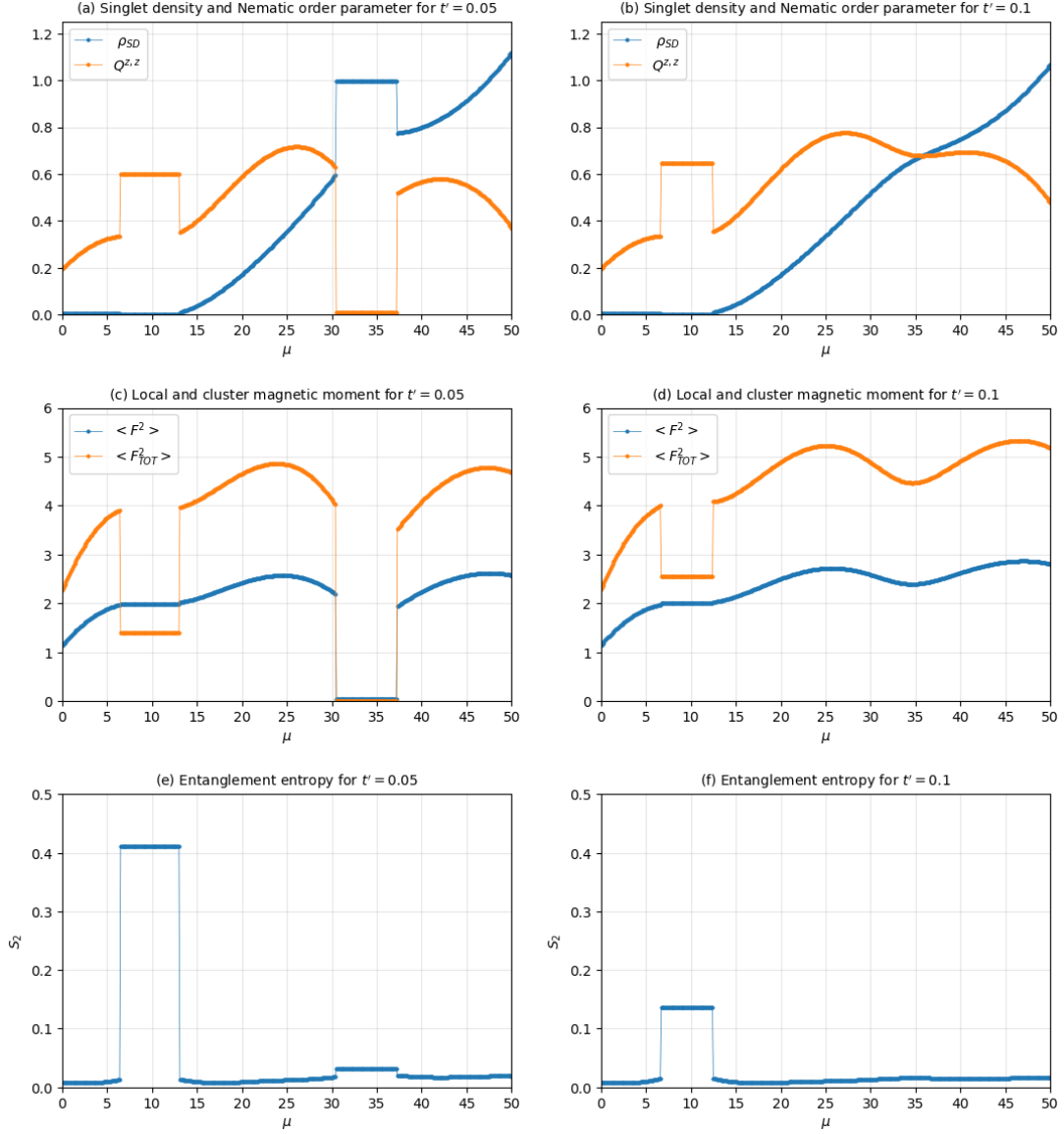


Figure 3.29: Comparison plots of singlet density  $\rho_{SD}$ , nematic order parameter  $Q^{z,z}$ , local magnetic moment  $\langle F^2 \rangle$ , cluster magnetic moment  $\langle F_{TOT}^2 \rangle$  and Rényi EE  $S_2$  against the chemical potential  $\mu$  for density-induced tunnelling amplitude  $t' = 0.05$  (left) and  $t' = 0.1$  (right) for  $U_2/U_0 = 0.03$  and  $U_0 = 24.0$ .

nematic order parameter is observed. The local magnetic moment  $\langle F^2 \rangle = 2$  in the  $\rho = 1$  MI phase for both DIT amplitudes. However, the global (cluster) magnetic moment  $\langle F_{TOT}^2 \rangle = 0$  only in the  $\rho = 2$  MI phase and is finite in the superfluid phases. An increase in the cluster magnetic moment is observed with DIT for the  $\rho = 1$  MI phase. From the plots of Rényi EE, it is observed that the entanglement entropy decreases as DIT amplitude increases. The discontinuous behaviour between the SF-MI phases continues in the calculated Rényi EE for both DIT amplitudes.

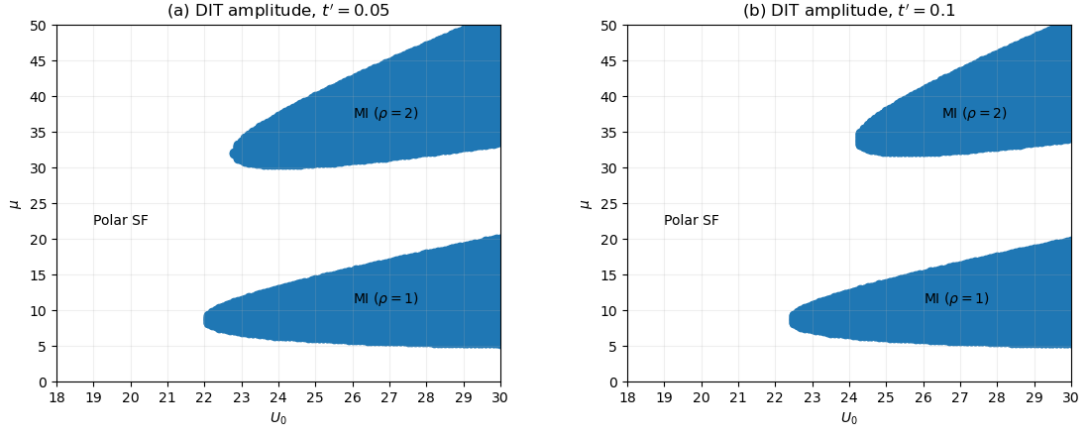


Figure 3.30: Phase diagram plots for  $U_2/U_0 = 0.03$  with density-induced tunnelling amplitude (a)  $t' = 0.05$  and (a)  $t' = 0.1$  for cluster size  $N_C = 2$ .

Lastly, the phase diagram plots at different density-induced tunneling amplitudes are plotted in figure (3.30) in the  $\mu - U_0$  plane. In contrast to the phase diagram obtained in figure (3.23), the polar superfluid region has widened while subsequently shrinking the MI phases. The impact of density-induced tunneling is more prominent as density of particles at a site increases.

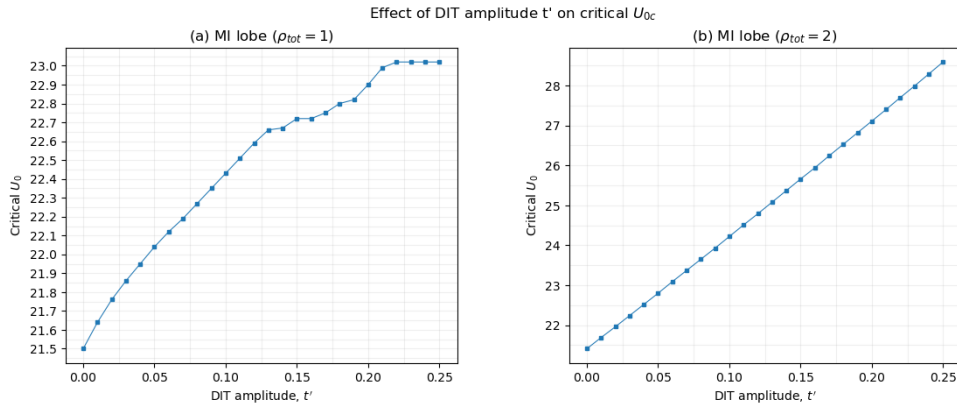


Figure 3.31: Effect of density-induced tunnelling amplitude  $t'$  on the critical  $U_0$  of Mott Insulator phases for  $U_2/U_0 = 0.03$  with cluster size  $N_C = 2$ .

To sum up the results obtained for the spin-1 BHM with DIT for cluster size  $N_C = 2$ , the graph of critical on-site interaction  $U_0^C$  against density-induced tunneling amplitude  $t'$  is plotted in figure (3.31). A near linear relation is seen for density  $\rho = 1$  MI lobe whereas the effect of shrinkage of the MI ( $\rho = 2$ ) lobe is seen to be linear with respect to density-induced tunneling amplitude.

### 3.2.3 Effect of finite temperature on Density-Induced Tunneling

Following the analysis of density-induced tunneling at zero temperature in the previous section, this section examines the effect of density-induced tunneling at finite temperatures.

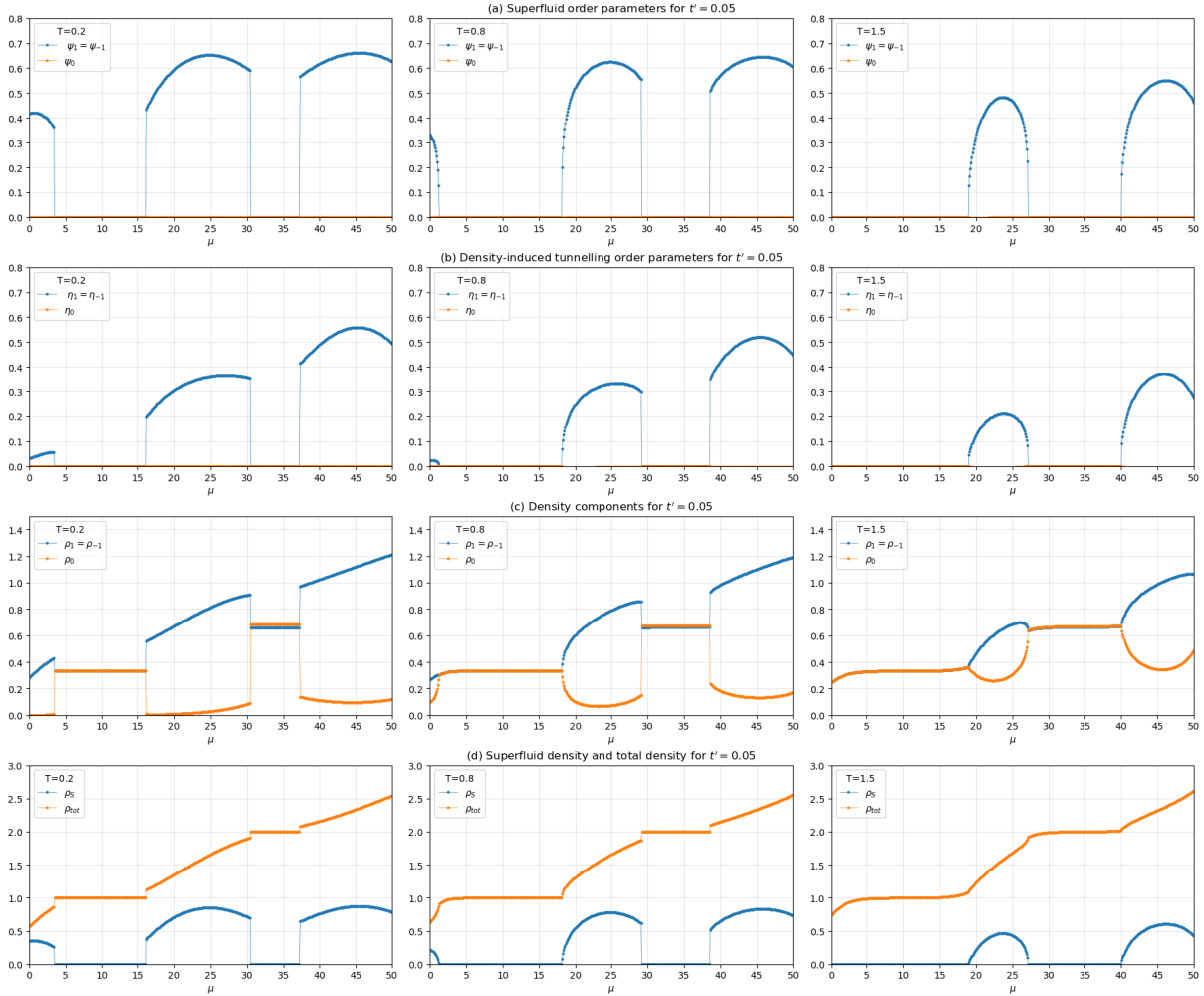


Figure 3.32: Comparison plots of superfluid order parameters  $\psi_\sigma$ , density-induced tunnelling order parameters  $\eta_\sigma$ , boson densities  $\rho_\sigma$  and superfluid density  $\rho_S$  and total density  $\rho_{tot}$  versus the chemical potential  $\mu$  for density-induced tunnelling strength  $t' = 0.05$  at temperatures  $T = 0.2$ ,  $T = 0.8$  and  $T = 1.5$  for  $U_2/U_0 = 0.03$  where  $U_0 = 24.0$ .

To study the effect of DIT and finite temperature on the two site Spin-1 BHM, the graphs in figure (3.32) and figure (3.33) are plotted for  $U_0 = 24.0$  and  $U_2/U_0 = 0.03$  at different temperatures for DIT amplitude  $t' = 0.05$  and  $t' = 0.1$  respectively.

At temperature  $T = 0$ , the polar nature of the superfluid phase is portrayed through the superfluid order parameters which take up values  $\psi_1 = \psi_{-1} \neq 0$  and  $\psi_0 = 0$ . This nature persists even at finite temperatures as seen in figure (3.32) and figure (3.33). The

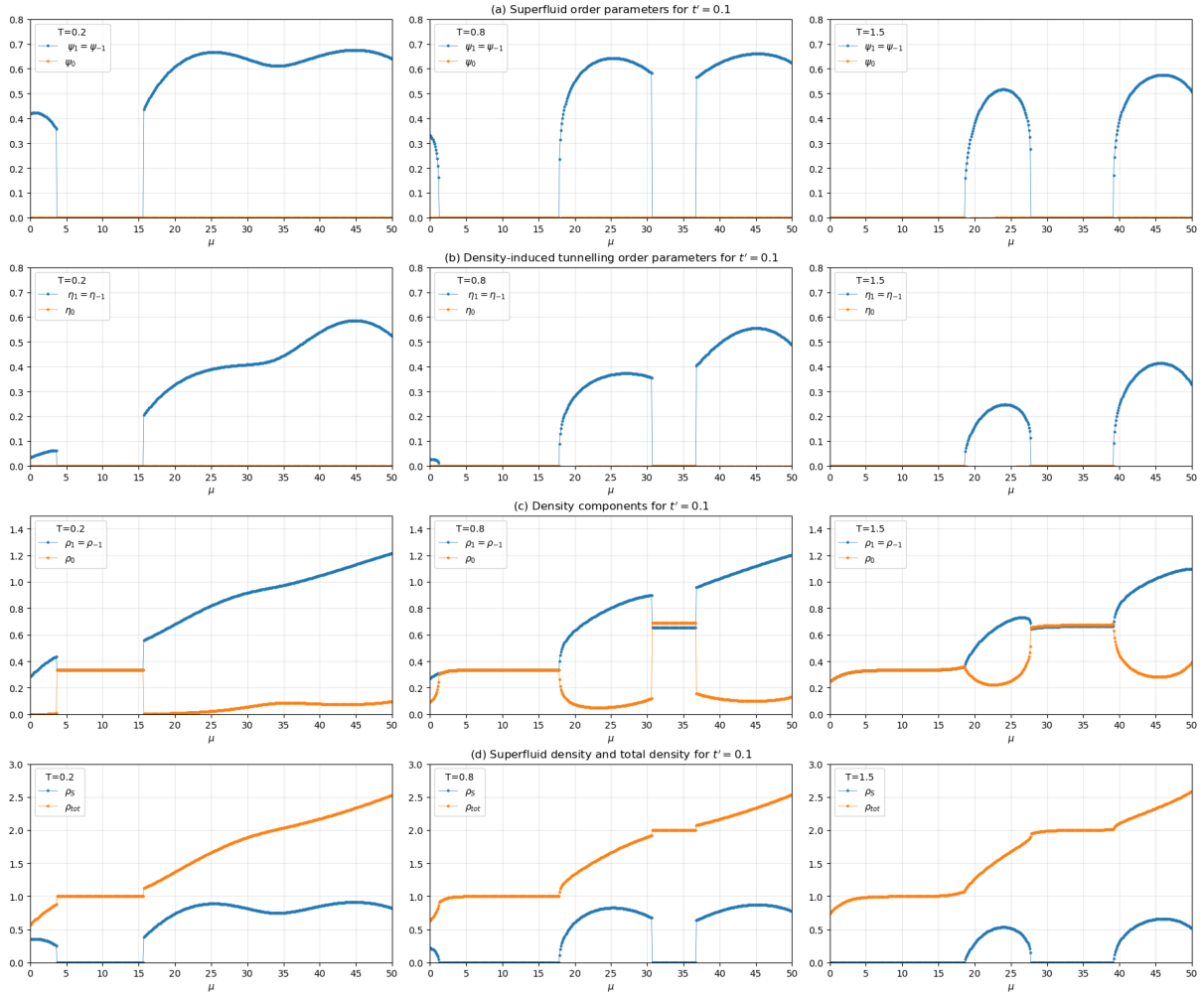


Figure 3.33: Comparison plots of superfluid order parameters  $\psi_\sigma$ , density-induced tunnelling order parameters  $\eta_\sigma$ , boson densities  $\rho_\sigma$  and superfluid density  $\rho_S$  and total density  $\rho_{tot}$  versus the chemical potential  $\mu$  for density-induced tunnelling strength  $t' = 0.1$  at temperatures  $T = 0.2$ ,  $T = 0.8$  and  $T = 1.5$  for  $U_2/U_0 = 0.03$  where  $U_0 = 24.0$ .

density-induced tunneling order parameters follow a similar nature like superfluid order parameters:  $\eta_1 = \eta_{-1} \neq 0$  and  $\eta_0 = 0$  in the superfluid phase and  $\eta_{0,\pm 1} = 0$  in the MI-NBL phase.

The density-induced tunnelling affects the Mott Insulator phase by increasing the superfluidity. For the same parameters plotted in figure (3.24), the MI ( $\rho = 2$ ) phase vanishes for DIT amplitude  $t' = 0.1$  for temperature  $T = 0.2$ . The other temperatures  $T = 0.8$  and  $T = 1.5$  see a visible reduction in the MI phases with a subsequent increase in the superfluid phase.

The discontinuous transition seen in these plots is due to thermal fluctuations that arise in the system due to finite temperatures. As temperature increases, the thermal fluctuations

become stronger and are sufficient to constantly overcome the energy barrier leading to a continuous phase transition.

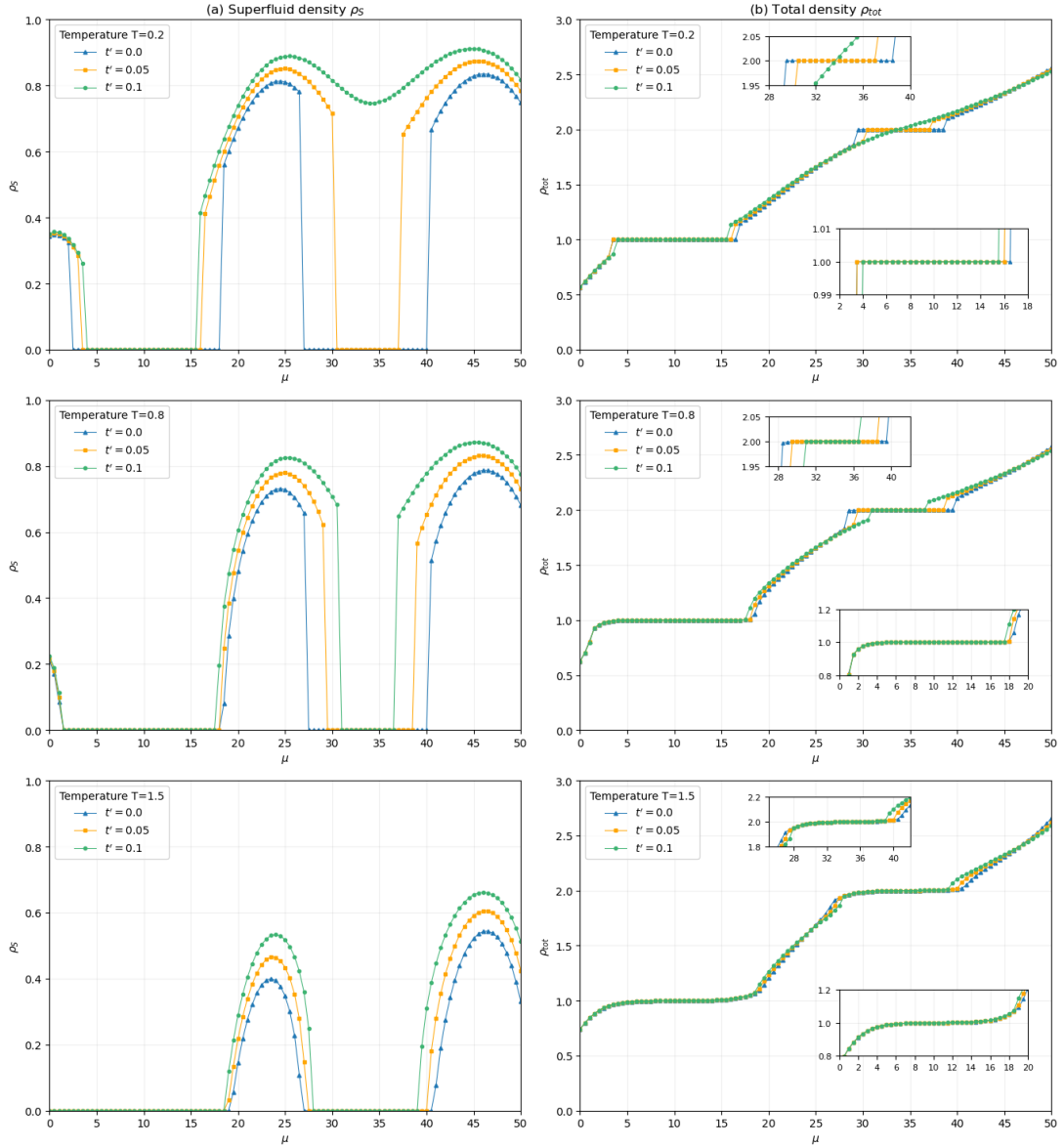


Figure 3.34: Comparison plots of (a) superfluid density  $\rho_S$  and (b) total density  $\rho_{tot}$  versus the chemical potential  $\mu$  for different density-induced tunnelling strengths at temperatures  $T = 0.2$ ,  $T = 0.8$  and  $T = 1.5$  for  $U_2/U_0 = 0.03$  where  $U_0 = 24.0$ .

The density contribution in MI ( $\rho = 1$ ) phase comes from all three components, that is,  $\rho_1 = \rho_0 = \rho_{-1} = 1/3$ . Similarly, the densities in the MI ( $\rho = 2$ ) phase are due to the three components, centered around  $2/3$ . The superfluid density and total density plots depict the transition from SF phase where  $\rho_S$  is finite to MI phase where  $\rho_S = 0$  and the density is fixed to an integer value at each site. However, at higher temperatures, the MI phase melts into the NBL phase where the compressibility is finite and particle density at a site

is not an integer.

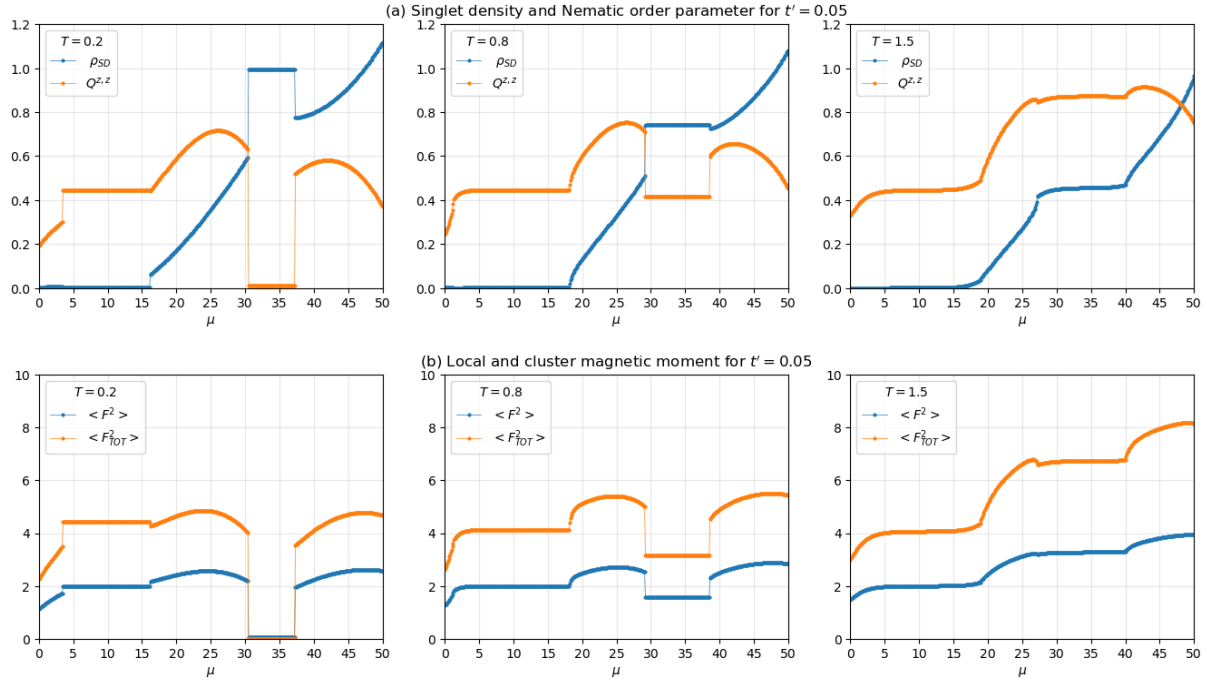


Figure 3.35: Comparison plots of (a) singlet density  $\rho_{SD}$  and nematic order parameter  $Q^{z,z}$  and (b) local magnetic moment  $\langle F^2 \rangle$  and cluster magnetic moment  $\langle F_{TOT}^2 \rangle$  versus the chemical potential  $\mu$  for temperatures  $T = 0.2$ ,  $T = 0.8$  and  $T = 1.5$  for density-induced tunnelling amplitude  $t' = 0.05$  for  $U_2/U_0 = 0.03$  and  $U_0 = 24.0$ .

A comparison between the superfluid densities for different density-induced tunneling amplitudes is done in figure (3.34). Similar comparison is carried out for the total densities for the same set of density-induced tunneling amplitudes in the same figure. The influence of density-induced tunneling is seen visibly through these plots. As density-induced tunneling amplitude is increased, superfluidity is enhanced and the MI phases get washed out. At a particular temperature, as the density-induced tunnelling amplitude increases, the Mott Insulator phase diminishes. Subsequently the superfluidity increases. However, at a given amplitude of density-induced tunnelling, as temperature increases, the Mott insulating phase increases.

Figure (3.35) and figure (3.36) represent the singlet density  $\rho_{SD}$ , nematic order parameter  $Q^{z,z}$ , local magnetic moment  $\langle F^2 \rangle$  and cluster magnetic moment  $\langle F_{TOT}^2 \rangle$  for temperatures  $T = 0.2$ ,  $T = 0.8$  and  $T = 1.5$  for density-induced tunnelling amplitudes  $t' = 0.05$  and  $t' = 0.1$  respectively. As temperature increases, the singlet pairs in the MI ( $\rho = 2$ ) phase start breaking due to thermal fluctuations and thus a decrease in the singlet density is observed. The nematic order parameter, local and cluster magnetic moment subsequently

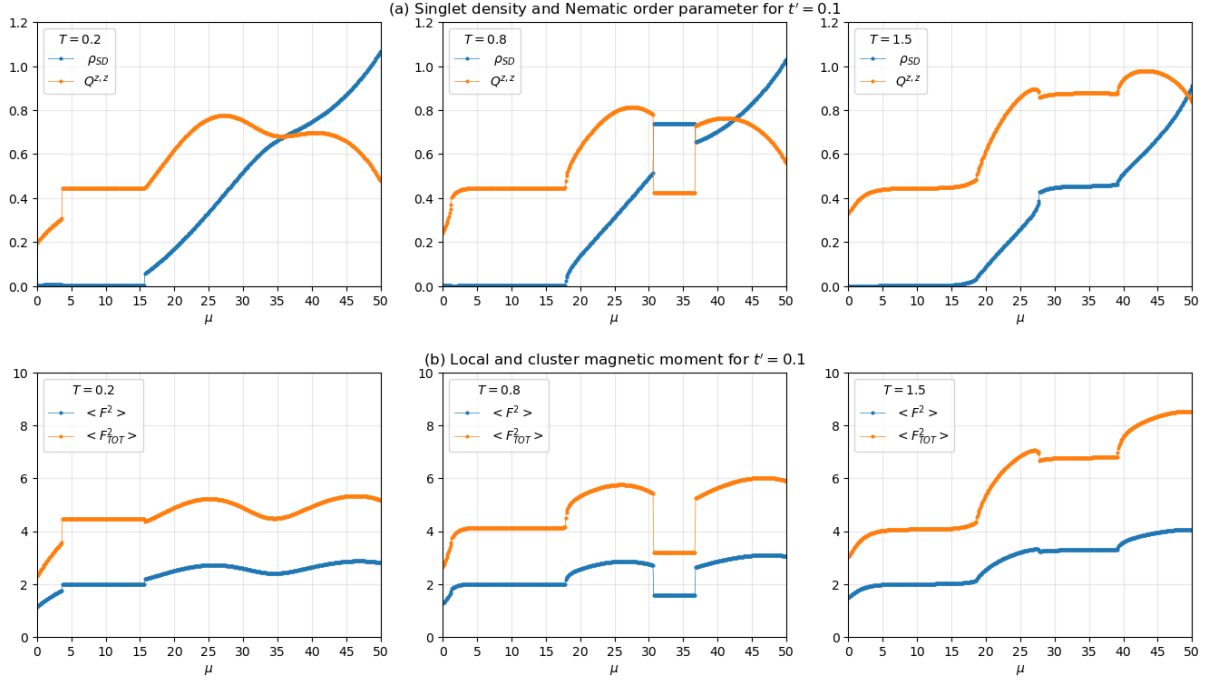


Figure 3.36: Comparison plots of (a) singlet density  $\rho_{SD}$  and nematic order parameter  $Q^{z,z}$  and (b) local magnetic moment  $\langle F^2 \rangle$  and cluster magnetic moment  $\langle F_{TOT}^2 \rangle$  versus the chemical potential  $\mu$  for temperatures  $T = 0.2$ ,  $T = 0.8$  and  $T = 1.5$  for density-induced tunnelling amplitude  $t' = 0.1$  for  $U_2/U_0 = 0.03$  and  $U_0 = 24.0$ .

increase since the antiferromagnetic arrangement can be easily broken by small thermal fluctuations. Thereby, the first order nature becomes continuous as temperature increases. A significant change wasn't observed in the MI ( $\rho = 1$ ) phase in these parameters. With the inclusion of density-induced tunnelling, the superfluidity increased leading to a decrease in the MI phases.

The phases arising due to finite temperature and DIT are emphasized in the phase diagrams in the  $\mu - T$  plane plotted for  $U_2/U_0 = 0.03$  and  $U_0 = 24.0$ . The plots in figure (3.37) and figure (3.38) illustrate the effect of density-induced tunnelling at finite temperatures. The superfluidity is seen to increase across both the phase diagrams and MI phases shrink. The compressibility is not affected by the inclusion of the density-induced tunnelling. The MI-NBL phase is a cross-over and the cross-over boundary is marked by cross-over compressibility  $\kappa = 0.005$ . It should be noted that this crossover boundary is not a strict phase boundary.

To conclude the results obtained for the spin-1 BHM with DIT at finite temperature for cluster size  $N_C = 2$ , the graph of critical on-site interaction  $U_0^C$  against density-induced

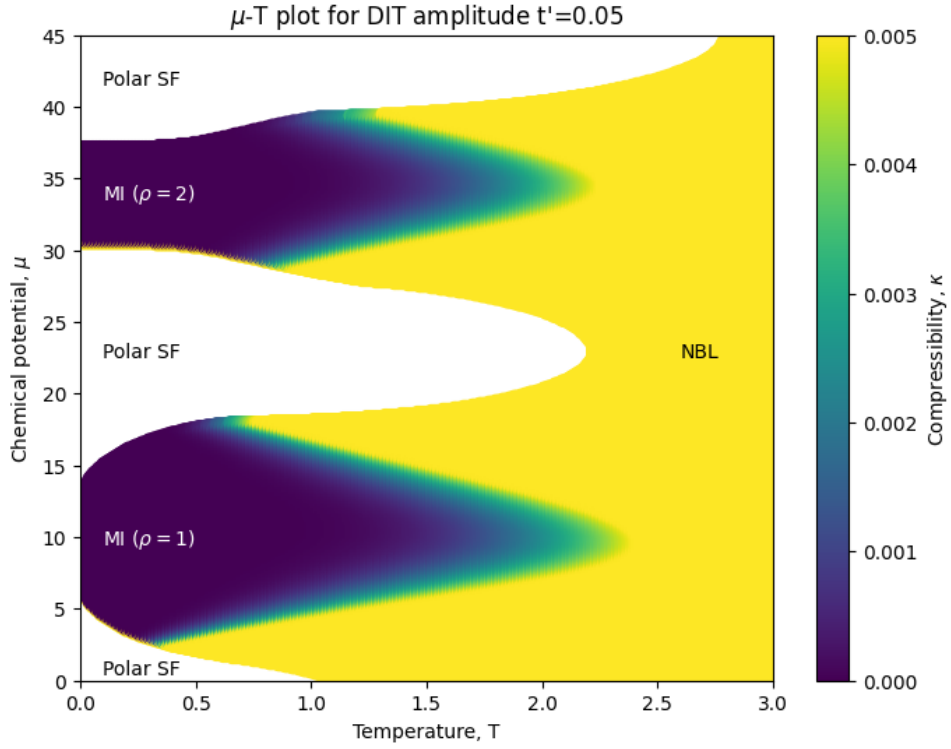


Figure 3.37: Chemical potential  $\mu$  versus temperature  $T$  plot with density-induced tunneling amplitude  $t' = 0.05$  for  $U_2/U_0 = 0.03$  and  $U_0 = 24.0$  for cluster size  $N_C = 2$ .

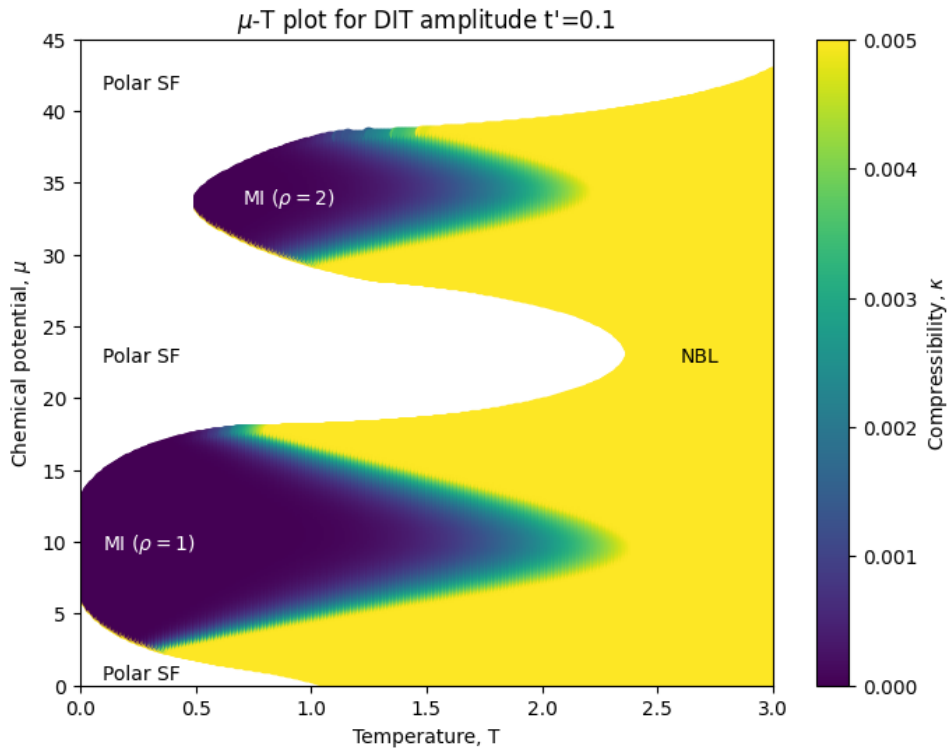


Figure 3.38: Chemical potential  $\mu$  versus temperature  $T$  plot with density-induced tunneling amplitude  $t' = 0.1$  for  $U_2/U_0 = 0.03$  and  $U_0 = 24.0$  for cluster size  $N_C = 2$ .

tunneling amplitude  $t'$  is plotted in figure (3.31). Both density  $\rho = 1$  MI lobe as well as the MI ( $\rho = 2$ ) lobes are seen to have a linear change in the critical  $U_0$  with respect to density-induced tunneling amplitude.

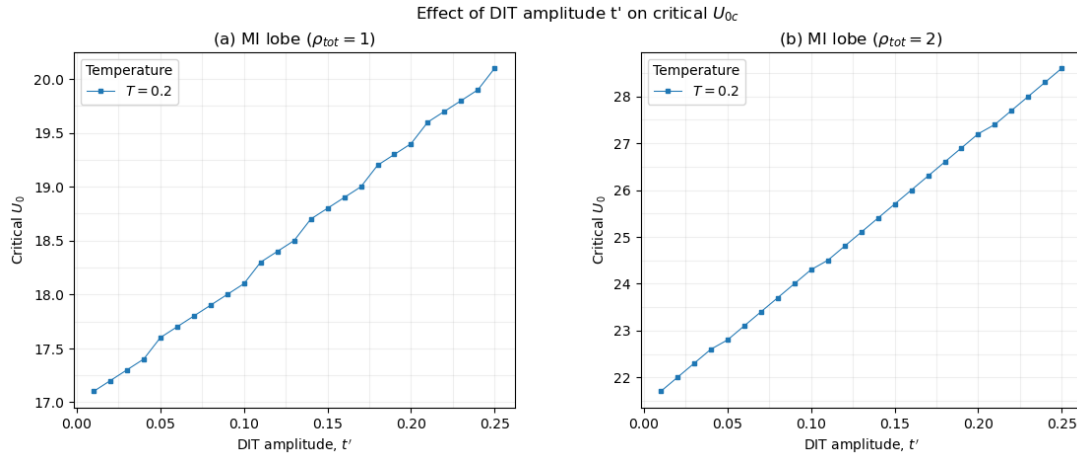


Figure 3.39: Effect of density-induced tunnelling amplitude  $t'$  on the critical  $U_0$  of Mott Insulator phases at finite temperature  $T = 0.2$  for  $U_2/U_0 = 0.03$  for cluster size  $N_C = 2$ .

# Chapter 4

## Conclusion

A finite temperature Cluster Mean Field Theory (CMFT) for a two-dimensional Spin-1 Bose Hubbard Model with Density-Induced Tunnelling (DIT) was developed. Cluster sizes up to two sites ( $1 \times 1, 2 \times 1$ ) were considered restricting the density  $\rho < 3$  ( $N_{max} = 3$ ). The analyses were carried out in the presence of spin-dependent antiferromagnetic interactions.

The single site ( $N_C = 1$ ) Mean Field Theory (MFT) showed qualitatively good results for the phase diagram of the spin-1 BHM with DIT. However, single-site MFT neglects fluctuations in the superfluid and Mott Insulator phases leading to an over-estimation of the critical on-site interaction  $U_0^C$ . In this regard, by employing Cluster Mean Field Theory (CMFT), the critical on-site interaction  $U_0^C$  decreased and the quantum fluctuations were incorporated well. The system was studied at finite temperatures and three phases were observed — Superfluid phase (SF), Mott Insulator phase (MI) and Normal Bose Liquid (NBL). The SF and MI phases melt into the NBL phase at high temperatures. The MI and NBL phases are cross-over phases for which the cross-over boundary was chosen as  $\kappa = 0.005$ .

The effect of the density-induced tunnelling term on the behaviour of the Spin-1 Bose Hubbard Model was studied. Enhanced superfluidity was observed with the inclusion of this term in the model Hamiltonian. The Mott Insulator lobes having higher filling factor were noted to be affected significantly. The impact of density-induced tunnelling along with finite temperatures was also studied for the Spin-1 Bose Hubbard Model. At a particular temperature, as the density-induced tunnelling amplitude increases, the

superfluidity increases leading to a decrease in MI phase. However, at a given amplitude of density-induced tunnelling, as temperature increases, the Mott insulating phase increases. The compressibility  $\kappa$  showed no change with density-induced tunnelling. Lastly, the effect of density-induced tunneling on the critical on-site interaction  $U_0^C$  was studied at zero and finite temperatures. The MI lobes were seen to shift linearly with an increase in DIT amplitude.

The present work can be extended to study the model for different values of spin-dependent antiferromagnetic interaction where  $0 < \frac{U_2}{U_0} < 0.5$ . A similar analysis can be carried out for the spin-dependent ferromagnetic interactions where  $-1 < \frac{U_2}{U_0} < 0$ . Here, positive values of the density-induced tunnelling amplitudes were studied. Following this, negative values of density-induced tunnelling amplitudes can be employed to study the novel phases arising in the model. The present work can also be extended to calculate the excitations, its spectral weights, and the density of states within a Random Phase Approximation (RPA) using standard basis operator method (SBO) [21].

# References

- [1] K. Aikawa, A. Frisch, M. Mark, S. Baier, A. Rietzler, R. Grimm, and F. Ferlaino. Bose-einstein condensation of erbium. *Phys. Rev. Lett.*, 108:210401, May 2012.
- [2] Bhargav K Alavani, Ananya Das, and Ramesh V Pai. Cluster mean field theory for two-dimensional spin-1 bose–hubbard model. *Journal of Physics B: Atomic, Molecular and Optical Physics*, 51(14):145302, 2018.
- [3] M. H. Anderson, J. R. Ensher, M. R. Matthews, C. E. Wieman, and E. A. Cornell. Observation of bose-einstein condensation in a dilute atomic vapor. *Science*, 269(5221):198–201, 1995.
- [4] Vesa Apaja and Olav F Syljuåsen. Dimerized ground state in the one-dimensional spin-1 boson hubbard model. *Physical Review A*, 74(3):035601, 2006.
- [5] G. G. Batrouni, V. Rousseau, R. T. Scalettar, M. Rigol, A. Muramatsu, P. J. H. Denteneer, and M. Troyer. Mott domains of bosons confined on optical lattices. *Phys. Rev. Lett.*, 89:117203, Aug 2002.
- [6] Ghassan George Batrouni, Richard T. Scalettar, and Gergely T. Zimanyi. Quantum critical phenomena in one-dimensional bose systems. *Phys. Rev. Lett.*, 65:1765–1768, Oct 1990.
- [7] Sara Bergkvist, Ian P McCulloch, and Anders Rosengren. Spinful bosons in an optical lattice. *Physical Review A*, 74(5):053419, 2006.
- [8] C. C. Bradley, C. A. Sackett, J. J. Tollett, and R. G. Hulet. Evidence of bose-einstein condensation in an atomic gas with attractive interactions. *Phys. Rev. Lett.*, 75:1687–1690, Aug 1995.

- [9] R. H. Chaviguri, T. Comparin, M. Di Liberto, and M. A. Caracanhas. Density-dependent hopping for ultracold atoms immersed in a bose-einstein-condensate vortex lattice. *Phys. Rev. A*, 97:023614, Feb 2018.
- [10] Jae-yoon Choi. Quantum simulations with ultracold atoms in optical lattices: past, present and future. *Journal of Korean Physical Society*, 82(9):875–881, May 2023.
- [11] K. B. Davis, M. O. Mewes, M. R. Andrews, N. J. van Druten, D. S. Durfee, D. M. Kurn, and W. Ketterle. Bose-einstein condensation in a gas of sodium atoms. *Phys. Rev. Lett.*, 75:3969–3973, Nov 1995.
- [12] L de Forges de Parny, F Hébert, VG Rousseau, and GG Batrouni. Interacting spin-1 bosons in a two-dimensional optical lattice. *Physical Review B*, 88(10):104509, 2013.
- [13] Eugene Demler and Fei Zhou. Spinor bosonic atoms in optical lattices: Symmetry breaking and fractionalization. *Phys. Rev. Lett.*, 88:163001, Apr 2002.
- [14] O Dutta, A Eckardt, P Hauke, B Malomed, and M Lewenstein. Bose–Hubbard model with occupation-dependent parameters - IOPscience. *New Journal of Physics*, 13(2), feb 9 2011.
- [15] Omjyoti Dutta, Mariusz Gajda, Philipp Hauke, Maciej Lewenstein, Dirk-Sören Lühmann, Boris A. Malomed, Tomasz Sowiński, and Jakub J. Zakrzewski. Non-standard hubbard models in optical lattices: a review. *Reports on Progress in Physics*, 78, 2014.
- [16] S. Ejima, H. Fehske, and F. Gebhard. Dynamic properties of the one-dimensional Bose-Hubbard model - IOPscience. *Europhysics Letters*, 93(3), feb 9 2011. [Online; accessed 2024-05-05].
- [17] Matthew P. A. Fisher, Peter B. Weichman, G. Grinstein, and Daniel S. Fisher. Boson localization and the superfluid-insulator transition. *Phys. Rev. B*, 40:546–570, Jul 1989.
- [18] Takeshi Fukuhara, Seiji Sugawa, and Yoshiro Takahashi. Bose-einstein condensation of an ytterbium isotope. *Phys. Rev. A*, 76:051604, Nov 2007.

- [19] Pallavi P. Gaude, Ananya Das, and Ramesh V. Pai. Cluster mean field plus density matrix renormalization theory for the Bose Hubbard models. *Journal of Physics A Mathematical General*, 55(26):265004, July 2022.
- [20] Markus Greiner and Simon Fölling. Optical lattices. *Nature*, 453(7196):736–738, jun 4 2008.
- [21] Stephen B. Haley and Paul Erdős. Standard-basis operator method in the green’s-function technique of many-body systems with an application to ferromagnetism. *Phys. Rev. B*, 5:1106–1119, Feb 1972.
- [22] AF Hincapie-F, R Franco, and J Silva-Valencia. Spin-1 bose–hubbard model with two-and three-body interactions. *Physics Letters A*, 382(26):1760–1765, 2018.
- [23] Tin-Lun Ho. Spinor bose condensates in optical traps. *Phys. Rev. Lett.*, 81:742–745, Jul 1998.
- [24] Adilet Imambekov, Mikhail Lukin, and Eugene Demler. Spin-exchange interactions of spin-one bosons in optical lattices: Singlet, nematic, and dimerized phases. *Physical Review A*, 68(6):063602, 2003.
- [25] D. Jaksch, C. Bruder, J. I. Cirac, C. W. Gardiner, and P. Zoller. Cold bosonic atoms in optical lattices. *Physical Review Letters*, 81(15):3108–3111, October 1998.
- [26] Dean Johnstone, Niclas Westerberg, Callum W. Duncan, and Patrik Öhberg. Staggered ground states in an optical lattice. *Phys. Rev. A*, 100:043614, Oct 2019.
- [27] Ole Jürgensen, Florian Meinert, Manfred J. Mark, Hanns-Christoph Nägerl, and Dirk-Sören Lühmann. Observation of density-induced tunneling. *Phys. Rev. Lett.*, 113:193003, Nov 2014.
- [28] Takashi Kimura. Strong-coupling expansion for the spin-1 bose-hubbard model. *Physical Review A*, 87(4):043624, 2013.
- [29] Takashi Kimura, Shunji Tsuchiya, Makoto Yamashita, and Susumu Kurihara. Superfluid–Mott Insulator Transition of Spin-1 Bosons in Optical Lattice under Mag-

- netic Field. *Journal of the Physical Society of Japan*, 75(7):074601–074601. [Online; accessed 2024-05-05].
- [30] Sebastian Kraft, Felix Vogt, Oliver Appel, Fritz Riehle, and Uwe Sterr. Bose-einstein condensation of alkaline earth atoms:  $^{40}\text{Ca}$ . *Phys. Rev. Lett.*, 103:130401, Sep 2009.
- [31] W. Krauth and N. Trivedi. Mott and Superfluid Transitions in a Strongly Interacting Lattice Boson System - IOPscience. *Europhysics Letters*, 14(7), apr 1 1991.
- [32] K. V. Krutitsky and R. Graham. Spin-1 bosons with coupled ground states in optical lattices. *Phys. Rev. A*, 70:063610, Dec 2004.
- [33] M. Landini, S. Roy, G. Roati, A. Simoni, M. Inguscio, G. Modugno, and M. Fattori. Direct evaporative cooling of  $^{39}\text{K}$  atoms to bose-einstein condensation. *Phys. Rev. A*, 86:033421, Sep 2012.
- [34] Dirk-Sören Lühmann, Ole Jürgensen, and Klaus Sengstock. Multi-orbital and density-induced tunneling of bosons in optical lattices - IOPscience. *New Journal of Physics*, 14(3), mar 13 2012.
- [35] T. McIntosh, P. Pisarski, R. J. Gooding, and E. Zaremba. Multisite mean-field theory for cold bosonic atoms in optical lattices. *Phys. Rev. A*, 86:013623, Jul 2012.
- [36] G. Modugno, G. Ferrari, G. Roati, R. J. Brecha, A. Simoni, and M. Inguscio. Bose-einstein condensation of potassium atoms by sympathetic cooling. *Science*, 294(5545):1320–1322, 2001.
- [37] Ramesh V Pai, K Sheshadri, and Rahul Pandit. Phases and transitions in the spin-1 bose-hubbard model: Systematics of a mean-field theory. *Physical Review B*, 77(1):014503, 2008.
- [38] Matteo Rizzi, Davide Rossini, Gabriele De Chiara, Simone Montangero, and Rosario Fazio. Phase diagram of spin-1 bosons on one-dimensional lattices. *Physical review letters*, 95(24):240404, 2005.
- [39] K. Sheshadri, H. R. Krishnamurthy, R. Pandit, and T. V. Ramakrishnan. Superfluid and Insulating Phases in an Interacting-Boson Model: Mean-Field Theory and the

- RPA - IOPscience. *Europhysics Letters*, 22(4), may 1 1993. [Online; accessed 2024-05-05].
- [40] D. M. Stamper-Kurn, M. R. Andrews, A. P. Chikkatur, S. Inouye, H.-J. Miesner, J. Stenger, and W. Ketterle. Optical confinement of a bose-einstein condensate. *Phys. Rev. Lett.*, 80:2027–2030, Mar 1998.
- [41] Simon Stellmer, Meng Khoon Tey, Bo Huang, Rudolf Grimm, and Florian Schreck. Bose-einstein condensation of strontium. *Phys. Rev. Lett.*, 103:200401, Nov 2009.
- [42] Yuta Toga, Hiroki Tsuchiura, Makoto Yamashita, Kensuke Inaba, and Hisatoshi Yokoyama. Mott transition and spin structures of spin-1 bosons in two-dimensional optical lattice at unit filling. *Journal of the Physical Society of Japan*, 81(6):063001, 2012.
- [43] Tao Wang and Tao Ying. Benchmark study of the SF-MI phase transition of the Bose-Hubbard model with density-induced tunneling. *Physics Letters A*, 383(7):680–683, February 2019.